RI 9106

Bureau of Mines Report of Investigations/1987

An Investigation of Crack Propagation With a Wedge Indenter To Improve Rock Fragmentation Efficiency

By D. A. Larson, R. J. Morrell, and J. F. Mades

UNITED STATES DEPARTMENT OF THE INTERIOR

Report of Investigations 9106

An Investigation of Crack Propagation With a Wedge Indenter To Improve Rock Fragmentation Efficiency

By D. A. Larson, R. J. Morrell, and J. F. Mades

UNITED STATES DEPARTMENT OF THE INTERIOR
Donald Paul Hodel, Secretary

BUREAU OF MINES
David S. Brown, Acting Director

Library of Congress Cataloging in Publication Data:

Larson, David A.
An investigation of crack propagation with a wedge indenter to improve rock fragmentation efficiency.

(Bureau of Mines report of investigations ; 9106)

Bibliography: p. **27.**

Supt. of Docs. no.: I 28.23: 9106.

1. Rocks–Fracture. 2. Rock splitters (Machines). I. Morrell, Roger J. II. Mades, J. (Joel F.). III. Title. IV. Series: Report of investigations (United States. Bureau of Mines) ; 9106.

TN23.U43 [QE431.6.M4] 622 s [622'.23] 87-600035

CONTENTS

ILLUSTRATIONS

ILLUSTRATIONS--Continued

TABLES

UNIT OF MEASURE ABBREVIATIONS USED IN THIS REPORT

in	inch	lb	pound (mass)
in·lbf	inch pound (force)	lbf	pound (force)
$in \cdot lbf/in^2$	inch pound (force) per square inch	lbf/in^2	pound (force) per square inch
in/min	inch per minute	lbf/in^3	pound (force) per cubic inch
min	minute	psi	pound (force) per square inch
pct	percent		

AN INVESTIGATION OF CRACK PROPAGATION WITH A WEDGE INDENTER TO IMPROVE ROCK FRAGMENTATION EFFICIENCY

By D. A Larson,[1] R. J. Morrell,[2] and J. F. Mades[3]

ABSTRACT

The Bureau of Mines conducted basic experiments to study the process of crack propagation with a wedge indenter. The work was conducted under plane stress conditions in a hard, brittle limestone. The purpose of these experiments was to first gain an understanding of the basic crack propagation process under a sharp indenter, and second, to determine how the crack propagation process could be used to improve mechanical fragmentation systems.

Three methods of rock fracture with the wedge indenter were investigated in this program. These were the confined indentation tests, the unconfined splitting tests, and the edge chipping tests. The confined indention tests represent worst case conditions for crack growth and formed the lower bound on fracture efficiency. The unconfined splitting tests represented best case conditions and fixed the upper bound of fracture efficiency. The edge chipping tests represented an idealized fragmentation process based exclusively upon the highly efficient fracture propagation process.

Edge chipping achieved a specific energy of 25 in·lbf/in^3 compared to conventional drag cutters, which required a specific energy of at least 2,385 in·lbf/in^3. Thus edge chipping is up to 100 times more efficient than conventional drag cutting. Because of these promising results, more work is planned with the fracture propagation process in three dimensions.

[1]Mining engineer.
[2]Supervisory mining engineer.
[3]Electronics engineer.
Twin Cities Research Center, Bureau of Mines, Minneapolis, MN.

INTRODUCTION

SCOPE

This research investigation is part of a continuing series of Bureau of Mines studies dealing with the mechanical fragmentation of rock. Previous efforts have investigated the development of more efficient mechanical fragmentation techniques such as the ripper-cutter and the drill-split systems (1-2).[4]

This report investigates rock fragmentation on a more basic level, utilizing the science of fracture mechanics. The work applies to both the experimental investigations mentioned previously and to other commercial mechanical fragmentation devices, such as tunnel boring machines, roadheaders, drills, etc.

The overall objective of this fragmentation research is to improve the efficiency and reduce the cost of mechanical fragmentation. This phase of the research investigated the fracture mechanics of the wedge-shaped indenter. The nearly universal use of the wedge indenter makes the results applicable to all major cutting systems, including drag bits and disk, button, and milled tooth cutters. The experiment was limited to two-dimensional plane stress conditions, a single bit geometry, and a single rock type, for simplicity. The independent variables of interest were the amount of confinement applied to the sample and the position of the wedge with respect to the free face. Because of the limited scope of these tests, the results and conclusions of this work must be considered preliminary.

LIMITATIONS OF CURRENT MECHANICAL FRAGMENTATION METHODS

In primary rock fragmentation, the only useful work is that done to remove a volume of rock from the solid mass. To be efficient, a minimum of new surface area should be created to break out a unit volume of rock. The creation of excess surface area consumes large amounts of energy while creating a problem with dust and fines.

Current methods of mechanical fragmentation, regardless of machine design or cutter type used, have cutters that travel in a fixed path. That is, the cutters are rigidly fixed to a cutterhead that itself moves in some fixed curvilinear path. The cutters, therefore, cannot move independently of the cutterhead to follow a plane of weakness or otherwise exploit some natural weakness in the rock mass. In addition, the individual cutters are unable to adjust their paths to compensate for the action of the adjacent cutters. The result of this cutting situation is that excessive crushing and fracturing is done in relation to the volume of rock removed.

For example, an analysis of the damage done to the rock surrounding the path of a drag cutter has been investigated by several researchers. Friedman (3) analyzed the fractures induced by a drag cutter in limestone and sandstone. Besides the fractures that ultimately formed rock chips, the cutter also formed two sets of fractures below the plane of the cutter and one set of fractures to the side of the cutter. These nonchip-forming fracture surfaces consume energy while contributing little to the actual material removal process. In addition, another source of energy waste was in the formation of gouge (fine-ground crushed rock) under the cutter.

Zeuch (4) also studied single drag cutters in granite and marble. Again, subsurface damage by the cutting process consisted of a set of fractures that dip at an angle in the direction of the motion of the bit and a set of fractures extending horizontally from the cut. Preliminary tests made in the presence of subsurface damage caused by prior cuts showed little influence on the cutting strength of rock. It was concluded that the energy adsorbed in producing the bottom and side fracture sets was not producing useful work.

[4]Underlined numbers in the parentheses refer to items in the list of references preceding the appendix.

Tutluoglu (5) calculated the surface area created during drag bit cutting and used the fracture surface energy to determine the total energy used to create chips. The useful energy was found to be approximately 8 pct of the total energy supplied to the bit. It was concluded that the remainder of the energy (>90 pct) must have gone into producing frictional heat. This waste heat creates high bit temperatures, which in turn lead to high rates of bit wear.

It is clear from these studies that current mechanical fragmentation methods are inefficient because of excessive crushing and frictional heat losses. What is needed is a process that would maximize the fractures that form chips while minimizing the bit-rock frictional contact between chips.

FRACTURE MODEL OF THE WEDGE INDENTER

An analysis of conventional mechanical cutter types shows that they involve a similar fragmentation process. Basically, some type of button or wedge is pushed into the rock to form chips. For example, rolling disk cutters are essentially a continuous wedge, while milled tooth or button cutters use many individual wedges or conical indenters. Even drag-type cutters can be modeled by the use of a wedge indenter moving through the rock, fracturing it in advance of the cutter (6). Given the universal application and importance of the wedge indenter, it was the shape selected for further study.

Studies of wedge indenters, including the prediction of crater depth and width as a function of the indenter geometry and applied load, are numerous and have been summarized by several researchers (7-8). These models do not, however, deal with the problem of crack initiation and crack propagation under the indenter and, hence, were not of immediate use to this study. Some of the most important studies of indentation fracture have been done by Lawn (9-10) and Swain (11). These authors divide indentation fracture into two parts, crack initiation and crack propagation. The sequence of fracture events for elastic, brittle rocks most applicable to this program, as given by Lawn, is shown in figure 1.

In figure 1*A* the point load is applied to the rock surface with a sharp indenter and a zone of crushed rock is formed; at 1*B*, as the load is increased the crushed zone increases until at some critical point a crack or cracks begins to extend out from this crushed zone; at 1*C*, as the load continues to increase the cracks propagate in a stable manner. The sequence 1*D* through 1*F* shows the unloading half of the cycle, which although not applicable to the process investigated, is shown for completeness. However, the lateral cracks that form during this unloading cycle may be related to the minor side chipping observed in Bureau tests. Consequently they will be discussed briefly in the indentation analysis portion of the "Identation Tests" section. The formation of the median vent or crack directly below the indenter is of primary importance to this report. The goal is to drive this type of crack to form a rock chip in a more energy efficient manner.

Therefore, the control of the second part of the fracture process, crack propagation, is of critical importance to any useful process. This part of the fracture process is under the influence of the stress field in the vicinity of the crack. Unfortunately, this stress field is not well known for the kind of complex geometries encountered in mechanical fragmentation systems. For this preliminary work, therefore, the energy balance method of Griffith (12) and Irwin (13) was used to predict the length of the cracks produced. This method is accurate for brittle materials where the amount of plastic deformation is small. The direction of the crack, however, cannot be predicted with certainty, but can be surmised from the shape of the general stress field in the path of the crack. The approach is considered adequate for this preliminary investigation, but future efforts will concentrate on defining the stress fields for more accurate results.

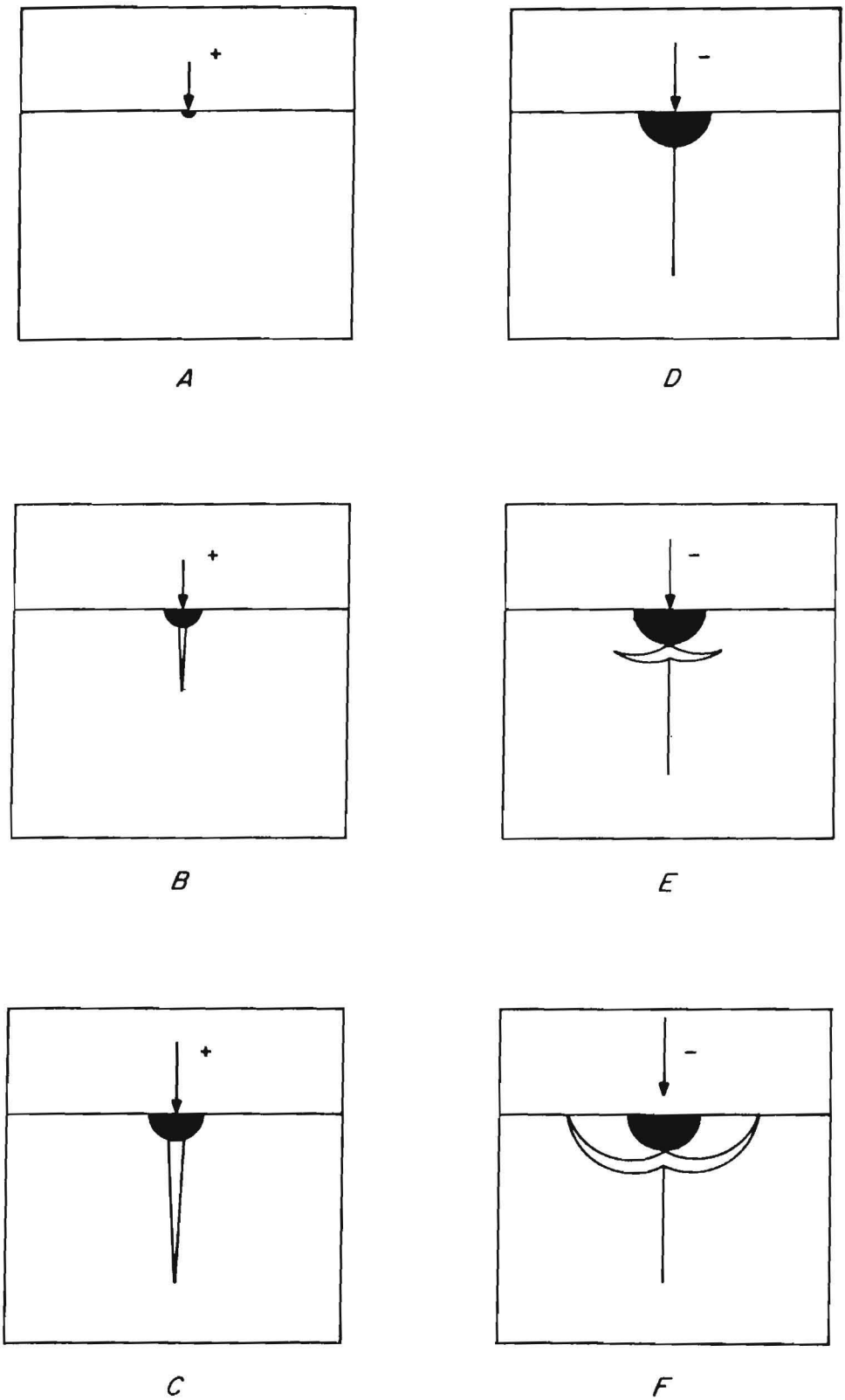

FIGURE 1.—Schematic of median crack formation under a point indenter. [Adapted from Lawn (*10*)]

EXPERIMENTAL EQUIPMENT

HIGH-STIFFNESS TESTING MACHINE

The indentation, splitting, and chipping tests were performed on a special Bureau-designed test apparatus called the crack propagation test device (CPTD) (fig. 2). This device was designed around a 400,000-lbf capacity compression testing machine to provide the adequate vertical and horizontal stiffness for a vertically moving bit. The two major components of concern of the compression machine are (1) four 37-in-long, 3-in-diam high-strength steel columns welded to 3-in-thick steel plates that are top and bottom reinforced with large channels and (2) an 8-in-diam bore hydraulic cylinder driven by a hand pump. A bit carriage made of channels, I-beams, steel round and plates, and concave rollers was designed to hold and vertically move a drag or indenter bit. The CPTD

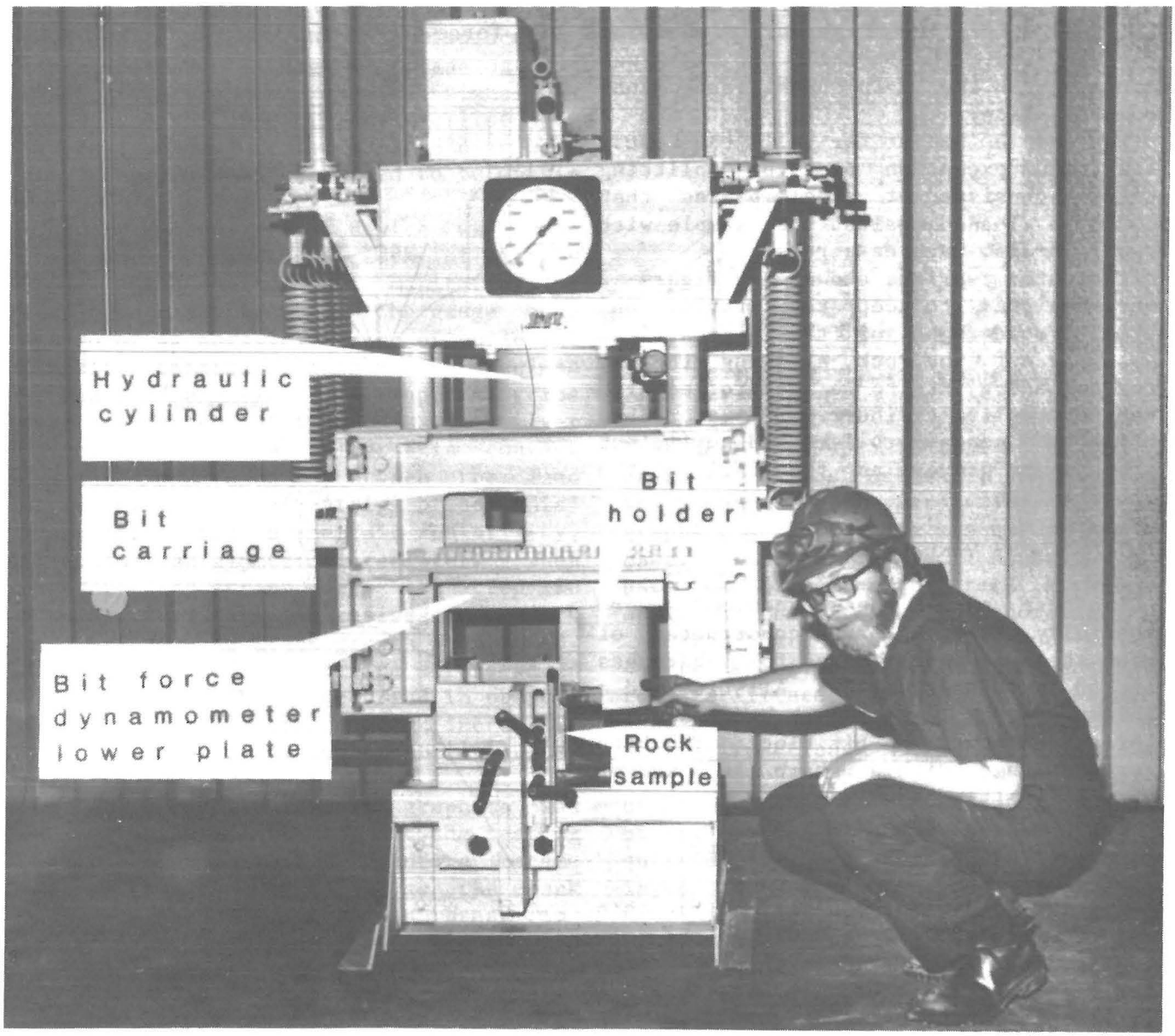

FIGURE 2.—Crack propagation device.

was designed to keep the system energy stored in the frame and hydraulic oil to a minimum so the crack propagation process could be stopped upon command. For the indenter tests reported here, the vertical system deformation was always less than 0.0004 in, with nearly half of that accounted for in the hydraulic oil. The horizontal deflection of the bit was always less than 0.0003 in, with one exception where it was nearly 0.003 in. The potential vertical energy never exceeded 1.4 in·lbf.

The bit holders, or bit blocks, were made from an 8-in round of steel. The bit holder in figure 2 shows the mounting for the bits. The indenter bit block was centered on the 2-in-thick force dynamometer plate.

The sample holder for all the tests, with the exception of the splitting tests, consisted of steel plates that could be loaded against the sample with two 1-in-diam machine screws.

The outer springs shown in figure 2 were designed to keep the gravity controlled deadweight of the bit-carriage assembly off the rock, allowing the bit force loading rate to be controlled with the hydraulic cylinder. However, as built, the concave rollers had sufficient preload to prevent any free fall of the bit carriage.

INDENTER BITS

The bits used in these experiments were specially designed and constructed of tool steel and heattreated to a hardness of 58 to 60 Rockwell C. All bits had a thickness of 1 in, and each had two holes for attaching to the bit block. The bits were designed with a sharp 40° wedge-shaped tip (fig 3).

TEST AND MEASUREMENT SYSTEM

Testing and data acquisition for this effort centered around obtaining the following data; applied horizontal-vertical forces, wedge displacement, and fracture growth (crack extension). All data were acquired versus time and fed into a four-channel digital oscilloscope where they were monitored, processed, and stored on a floppy disk. From these measurements, force-energy versus displacement and force-energy versus crack extension were computed, plotted, and stored.

Commercially built force washers were combined to create two force channels, F1F2 (channel 1) and F3F4 (channel 2) (fig. 4). All force washers were preloaded to permit the monitoring of force magnitude as well as force direction. Both channels passed through signal conditioners before arriving at the digital scope. The channels were then combined, by addition to obtain vertical force, and by subtraction to obtain the horizontal force. Upon calibration, full-scale

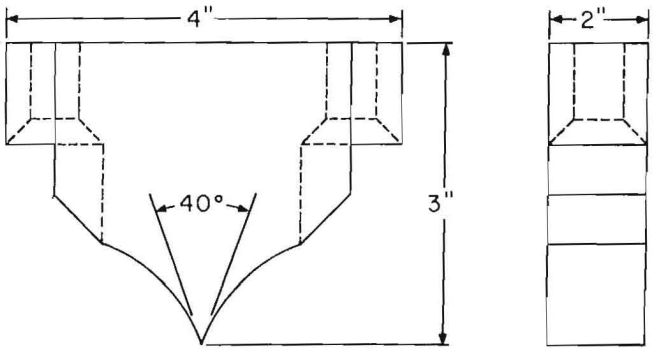

FIGURE 3.—Indenter bit.

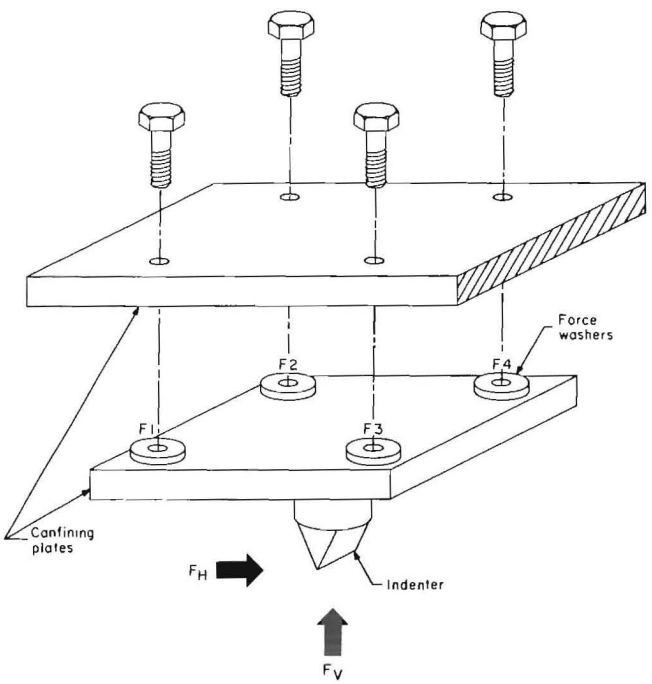

FIGURE 4.—General layout of force washers, confining plates, and indenter.

accuracies were found to be within ±1.7 pct and ±2.5 pct for vertical and horizontal force, respectively. Cross-talk was no greater than ±1.8 pct of full scale.

Bit position data were acquired using an optical encoder as the primary measuring element. Since the incremental encoder outputs two square waves in quadrature, both distance and direction information could be determined. Linear motion of the bit was translated to the rotary encoder by means of a shaft-mounted pully-cable device. From the quadrature waveforms, a binary 12-bit up-down count, proportional to displacement was generated. A digital-to-analog conversion was performed and the signal was interfaced to the digital oscilloscope. Calibration was performed and displacement accuracy was determined to be within ±0.0008-in.

A crack propagation device was constructed, based on the work of Smirnov (14), which enabled the monitoring of real-time crack growth. The gauge consisted of 41 parallel strips of colloidal graphite painted onto the test specimen by means of a mask. The graphite strips were connected at the ends by silver paint. A flexible silver skin contact compound was used to attach the lead wires (fig. 5). A strip of collodial graphite, having a certain resistivity, simulates an electrical resistor. When the graphite strips were connected in parallel, a parallel-resistance network was formed. As crack growth progressed, consecutive colloidal strips were severed and resistance change occurred in proportion to crack length. Crack increments in 0.050-in strips, up to 6-in length, could be monitored.

A water-based colloidal graphite was chosen, which effectively met the testing needs. The colloidal graphite became very brittle when dried, so as the crack passed through it, it would break immediately. The crack propagation gauge was incorporated into a Wheatstone quarter-bridge configuration. By adding the proper parallel and series resistances to the circuit, a repeatable voltage change would occur each time the gauge was severed.

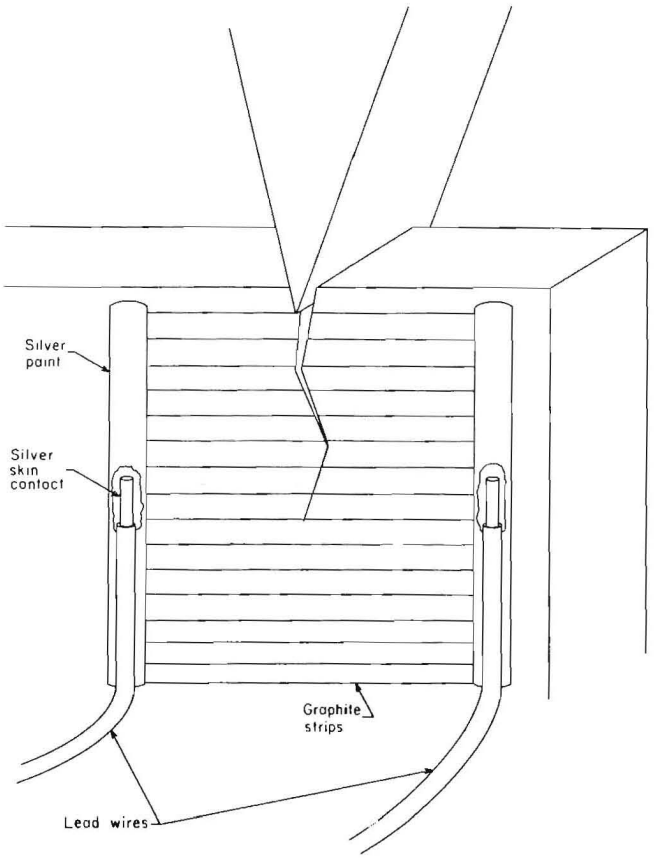

FIGURE 5.—Crack propagation gauge.

It must be kept in mind that for the gauge to be most accurate, crack growth was assumed to be perpendicular to the graphite strips. This was not always the case. The best one could do was anticipate the direction of crack growth and apply the graphite strips accordingly.

At the heart of the test setup was the digital oscilloscope. This essential tool facilitated rapid data and waveform acquisition, evaluation, printout, and storage functions. The flexibility and versatility of the digital scope was also of great benefit in meeting the demands of the varied and complex testing requirements. The overall test equipment layout is shown in figure 6.

ROCK SAMPLE

The rock used for all testing was a hard, fine-grained dolomite, locally known as Valders white rock. This rock was chosen because of its fine-grained texture and because its properties and

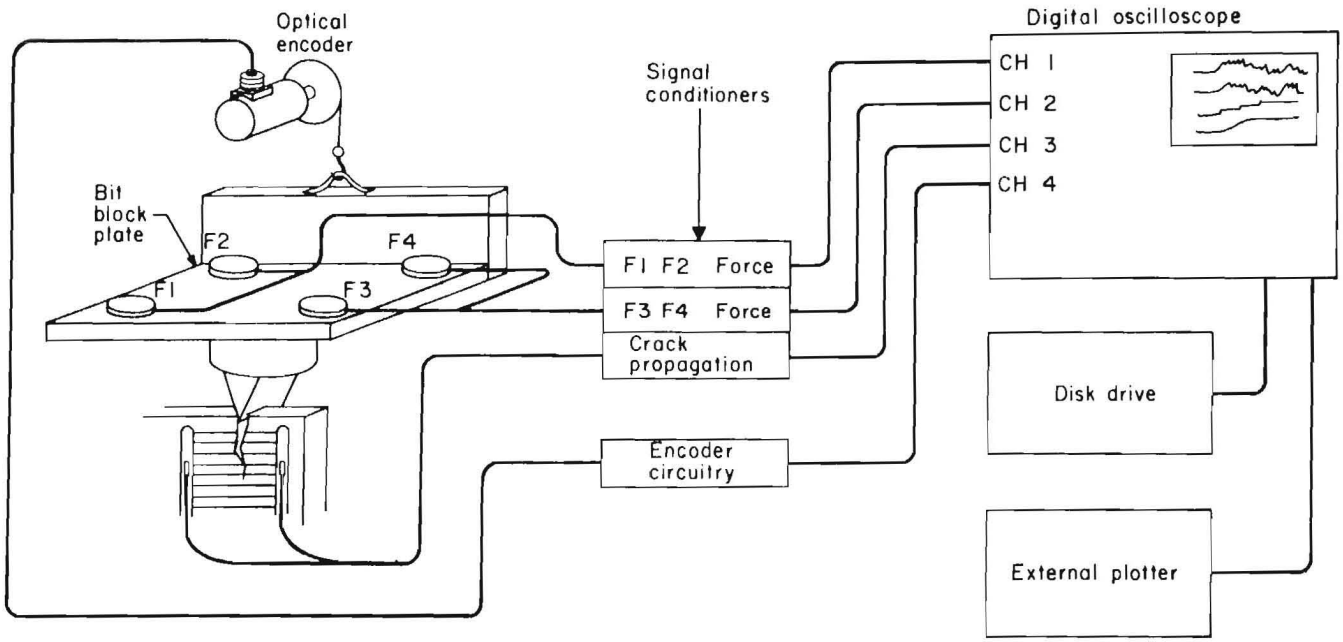

FIGURE 6.—Test equipment layout.

TABLE 1. - Chemical analyses of Valders dolomite, percent

Component	
SiO_2	30.1
CO_2	26.7
CaO	16.5
MgO	15.1
Al_2O_3	1.1
K_2O	.96
Na_2O	.11
H_2O	5.3
Undetermined	4.1

TABLE 2. - Physical properties of Valders dolomite[1]

Fracture surface energy (15) in·lbf/in^2	0.25
Compressive strength....lbf/in^2	27,230
Tensile strength.....lbf/in^2	793
Static Young's modulus 10^6 lbf/in^2	5.7
Poisson's ratio	0.20

[1]Geologic name: Cordell dolomite member, manistique formation; commercial name: Valders white rock; locality: Valders, WI.

fragmentation characteristics were known from previous tests. Its chemical composition and physical properties are given in tables 1 and 2. The high silica content along with its fine grain structure makes it a highly brittle rock. The rock contained no open defects or structure, but did contain some slight, discontinuous bands of color. These color bands were thought to represent a remnant of a past physical structure, and all testing was done perpendicular to the bands for consistency. The rock was cut into 6- by 6- by 1-in pieces for testing, and the larger surfaces were ground smooth to aid in observing the crack growth.

INDENTATION TESTS

The first series of tests performed in this program were the indentation tests. The indenter was applied to the edge of a flat sample, remote from the corners or other free surfaces that might aid the fracturing process. The flat-plate sample was confined on the ends to simulate a two-dimensional semi-infinite rock mass. Because of the confinement and the lack of any other free face or edge to

aid crack growth, these tests represent worst case conditions to crack growth and form the lower limit of fracture efficiency for mechanical indenters. Of primary interest in these experiments was the overall sequence of events leading to crack growth, the relationship between crack length and applied force, and the energy efficiency of the process.

EXPERIMENTAL PROCEDURE

The 6- by 6- by 1-in-thick rock samples were oriented with bedding horizontal and centered beneath the 40° wedge indenter. The samples were confined on the ends to simulate a 1-in-thick plate of semi-infinite length. The sample's confining load was cushioned with thin (<0.02-in) firm cardboard to avoid stress concentrations. One side was backed by several inches of steel plate and the other side had at least 2 in of steel plates with two 1-in screws applying a 600-lbf load each (fig. 7).

During testing the loading rate was maintained at approximately 0.02 in/min to allow observation of slow crack propagation. The average test duration was about 6 min, and total wedge displacement was approximately 0.1 in. The forces, displacement, and crack extension were monitored. A typical plot of vertical force and energy for an indentation test are shown in figure 8.

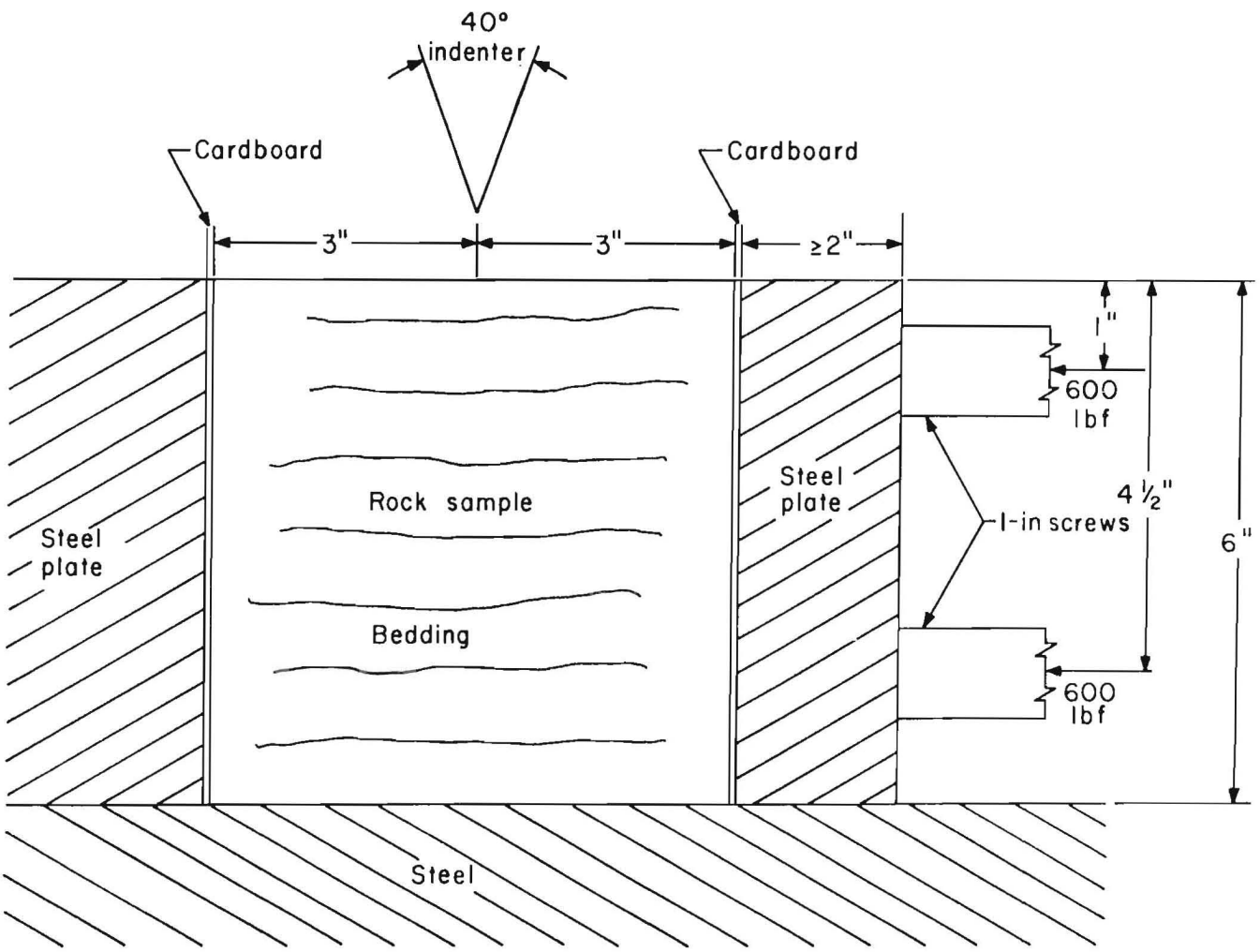

FIGURE 7.—Rock sample position and confinement for indentation tests.

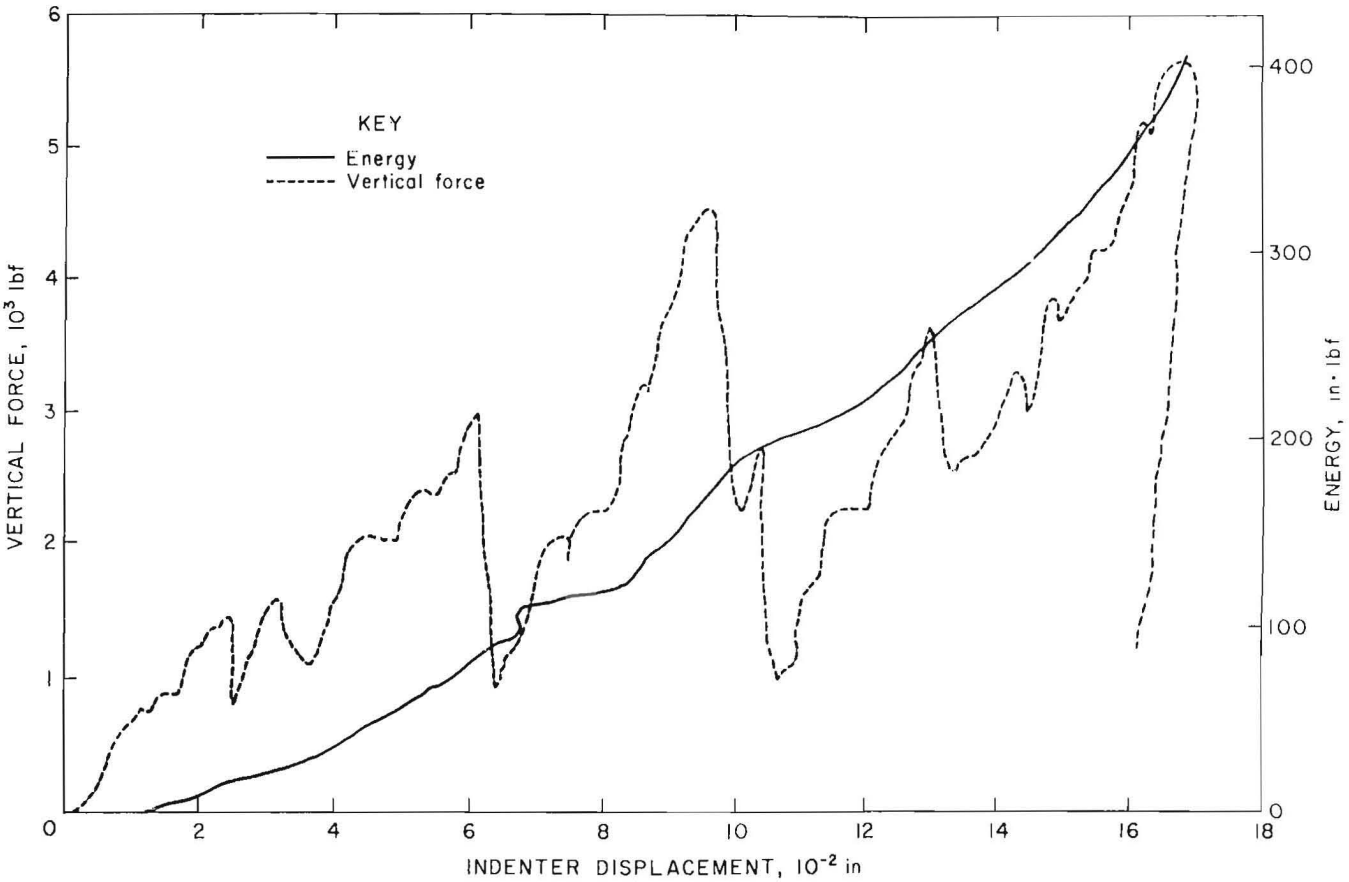

FIGURE 8.—Typical vertical force and energy plot for an indentation test.

EXPERIMENTAL RESULTS

The first result from these tests was the overall sequence of the crack initiation and propagation process. Basically the process starts with a crushed zone that is formed directly under the edge of the indenter. This crushed zone formed almost immediately and continued to form, up to the point of maximum applied load, after which it stabilized for the remainder of the tests. As the load is increased, this crushed zone increases until a crack forms out of it. The crack could not be detected until it reached a length of 0.25 in or more, which coincided to a wedge load of about 4,000 lbf and a displacement of 0.09 in. As the indenter continues into the rock, this crack grows in a stable manner. The length of crack that could be grown in a stable manner varied from 2 to 6 in. The length depended on the amount of confinement stress applied to the sample, with the higher confinement stresses creating the more unstable crack propagation conditions.

This sequence of events essentially confirms the model presented by Lawn (10) shown in figure 1. The only major difference in the present work was the additional formation of small chips, which formed to each side of the indenter. These side chips formed in discrete jumps as the load built to a high value. When the chips formed, the indenter was unloaded and the force dropped. This process continued throughout the tests and gave rise to the force of fluctuations shown in figure 8.

The final result of each test was the formation of a crater, with a zone of crushed material at the bottom and a crack emanating downward from this

crushed zone. The side chips that formed during this process may be related to the lateral cracks formed during the unloading sequence as shown in figure 1. These lateral cracks, according to Swain (11), form when the indenter is unloaded from the sample, whereas in the present work the side chips are formed when the load is at a maximum and the indenter is unloaded because of the formation of lateral chips.

Many investigators (7 8) have studied this side chipping phenomenon and it forms the basis of many existing rock cutting systems. However, in the present work these lateral cracks, and the side chips they create, are of little practical value because of the very small volume of rock removed (<1 pct) as compared to the volume removed by the major chipping process. Therefore, these side chips and lateral cracking will not be discussed further in this report.

The second important result from the tests is the relationship between indenter force and crack length (fig. 9). Crack length data were collected between 0.5 in and 2.0 in, since cracks less than 0.5 in could not be detected and cracks larger than 2.0 in could not be controlled. Front surface spalling of the 1-in-thick rock slabs near the indenter eliminated the detection of short crack lengths. The crack growth was monitored optically and the colloidal graphite gauge output was used primarily as a check on the results. The colloidal gauges were generally successful, but the output tended to lead or lag the optically recorded crack length probably because of the nonhomogeneity of the rock. The crack path was essentially straight for all of the tests except for slight undulations thought to be caused by variations in the rock itself.

The dashed line (fig. 9) represents the theoretical prediction line and will be discussed in the following analysis section. The data show that beyond a crack length of about 0.5 in, the force required to propagate the crack steadily decreases. Alternatively, crack length is a function of the square of the indenter load, again showing the advantages of the later stages of crack growth. These tests show that subsurface cracks

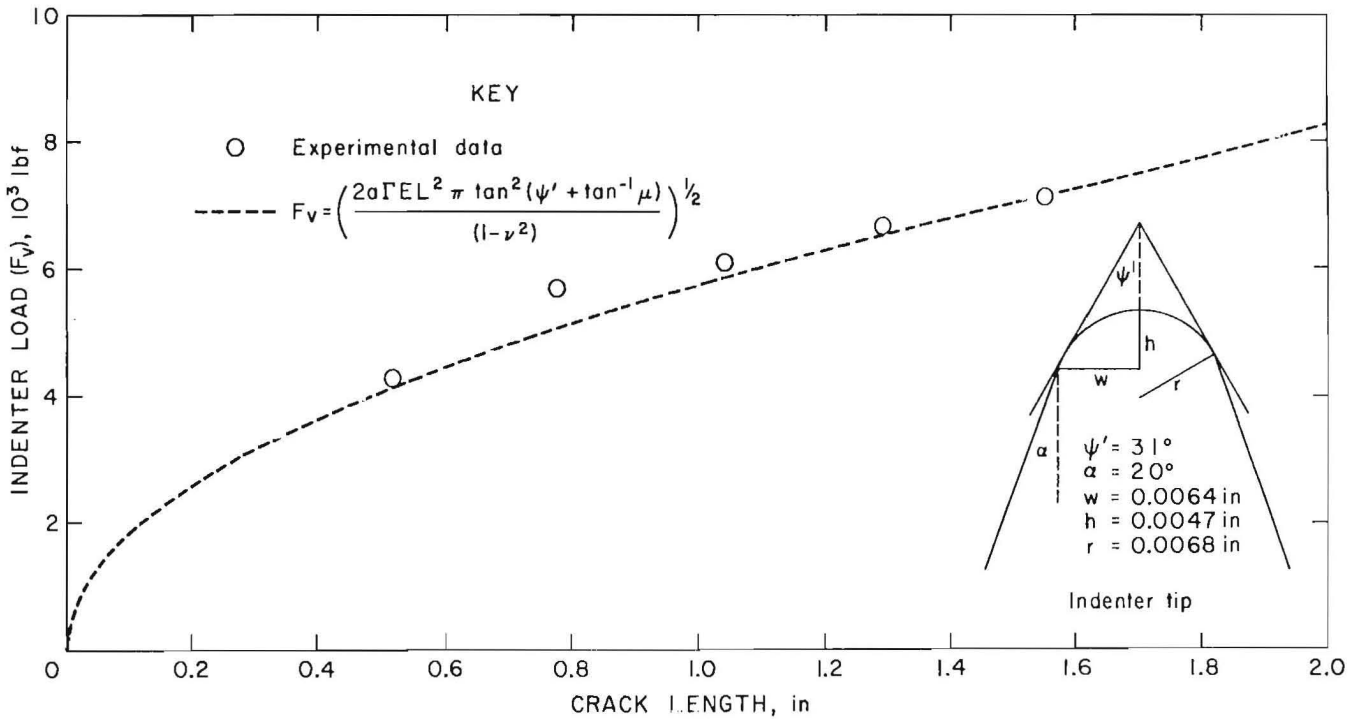

FIGURE 9.- Fracture mechanics relationships for 40° indentation test data in Valders dolomite. [Equation from Swain (*11*)]

form directly under sharp indenters in a confined rock mass and that the length of these cracks is a function of indenter load. All of the cracks observed in these tests were the median-type vents as shown in figure 1.

The final result of interest is the energy efficiency of the fracturing process. Figure 10 shows the apparent specific fracture surface energy as a function of crack length interval. Specific fracture surface energy is defined as the energy required to create a unit area of new fracture surface. Figure 10 clearly shows that energy requirements are high in the early stages of crack growth. This is a result of the need to deform and crush the rock under the indenter to initiate the crack. The data show that about 90 pct of the total energy is used to initiate and drive the crack the first 1-in and the remaining 10 pct is used to drive the crack from 1 to 3 in. The best specific energy achieved in the later stages of growth was 5.8 in·lbf/in^2, which compares well to the fracture surface energy of the rock of 0.25 in·lbf/in^2. Thus, even confined indentation, which is the worst case condition for crack growth, achieves very low specific fracture energies when the crack is in its well-developed stage.

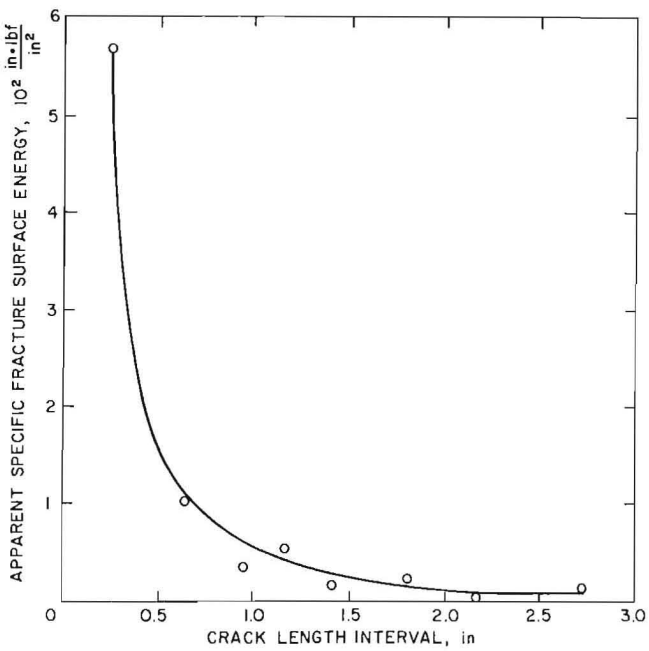

FIGURE 10.—Apparent specific fracture surface energy as a function of crack length interval for the identation tests.

INDENTER ANALYSIS

Basic to the understanding of the crack growth phenomenon under an indenter is a knowledge of the relationship between crack length and indenter load, indenter geometry, and the physical properties of the rock. With this knowledge, the effect of changes in indenter geometry or rock properties can be analyzed to predict either crack length or indenter load. The relationship of interest has been analyzed by Swain (11).

The approach used by Swain is to equate the change in mechanical energy to the change in surface energy as a crack is extended. This is the Griffith-Irwin energy balance for crack equilibrium (12-13). The change in surface energy is proportional to

$$\delta U_s \propto \Gamma L \delta a, \qquad (1)$$

where δU_s = change in surface energy, in·lbf.

Γ = fracture surface energy, in·lbf/in^2.

L = length of indenter, in.

and δa = change in crack length, in.

The change in mechanical energy is given by

$$\delta U_m \propto -F_v^2 \, \delta a / La \, E, \qquad (2)$$

where δU_m = change in mechanical energy, in·lbf,

F_v = indenter load, lbf,

a = crack length, in,

and E = Young's modulus (lb^6/in^2)

Equating the change in surface energy, U_s, to the change in mechanical energy, U_m, and solving for the crack length gives

$$a = K_L F_v^2/2\Gamma EL^2 \quad (3)$$

and $$K_L = (1 - \nu^2)/\pi \tan^2 \Psi, \quad (4)$$

where K_L = dimensionless constant accounting for the geometry of the sharp wedge indenter,

ν = Poission's ratio,

and $\Psi = \Psi' + \tan^{-1} \mu$,

where Ψ' = half angle of sharp wedge indenter,

and μ = coefficient of sliding friction.

Using equation 3, the theoretical curve has a difference no greater than 15 pct from the data curve. It appears that equation 3 is a reasonable predictor for the crack propagation (fig. 9). However, there are insufficient data to make any statement about the crack initiation process. The half angle, Ψ', was measured at 31° because aftertest microscopic examination of the tip of the indenter showed a tip radius of curvative of less than 0.0068 in with chord length of 0.0129 in at the arc intersection and the inclined straight sides of the indenter (fig. 9). The coefficient of friction was assumed to 0.6 (16) because of the very slow indenter displacement rate, approximately 0.02 in/min.

The value of this confined indenting work is that it shows that a single, well-developed crack extends beneath the tip of a wedge-shaped indenter and that this crack grows as a function of indenter load in a well defined manner. The absolute values of F_v/a are a function of material properties and indenter geometry and will be different for each bit and rock type tested. The use of this well-defined crack will be exploited in a succeeding section to develop an improved chip formation process.

SPLITTING TESTS

The second series of tests performed in this program were the splitting tests. In these tests, the wedge indenter was applied to the edge of a flat sample that was not confined in any way. These tests represent the best case conditions for crack growth and form the upper limit of efficiency for indenter type bits. Of primary interest in these tests is the relationship between crack length and indenter load and the energy efficiency of the fracturing process.

EXPERIMENTAL PROCEDURE

The 6- by 6- by 1-in-thick rock samples were oriented with the bedding horizontal and centered beneath the 40° wedge indenter. The samples were placed on 1/2-in rollers to eliminate the frictional confinement on the bottom edge due to the indenter load (fig. 11).

During testing, the loading rate was maintained at approximately 0.02 in/min to allow observation of slow crack propagation. The average test duration was about 6 min. The forces, displacement, and crack extension were monitored.

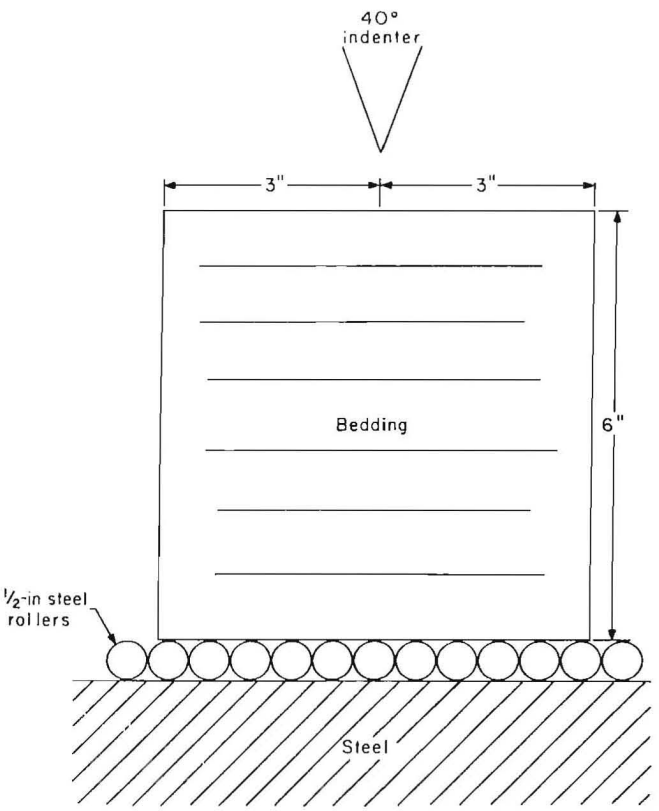

FIGURE 11.—Sample setup for splitting tests.

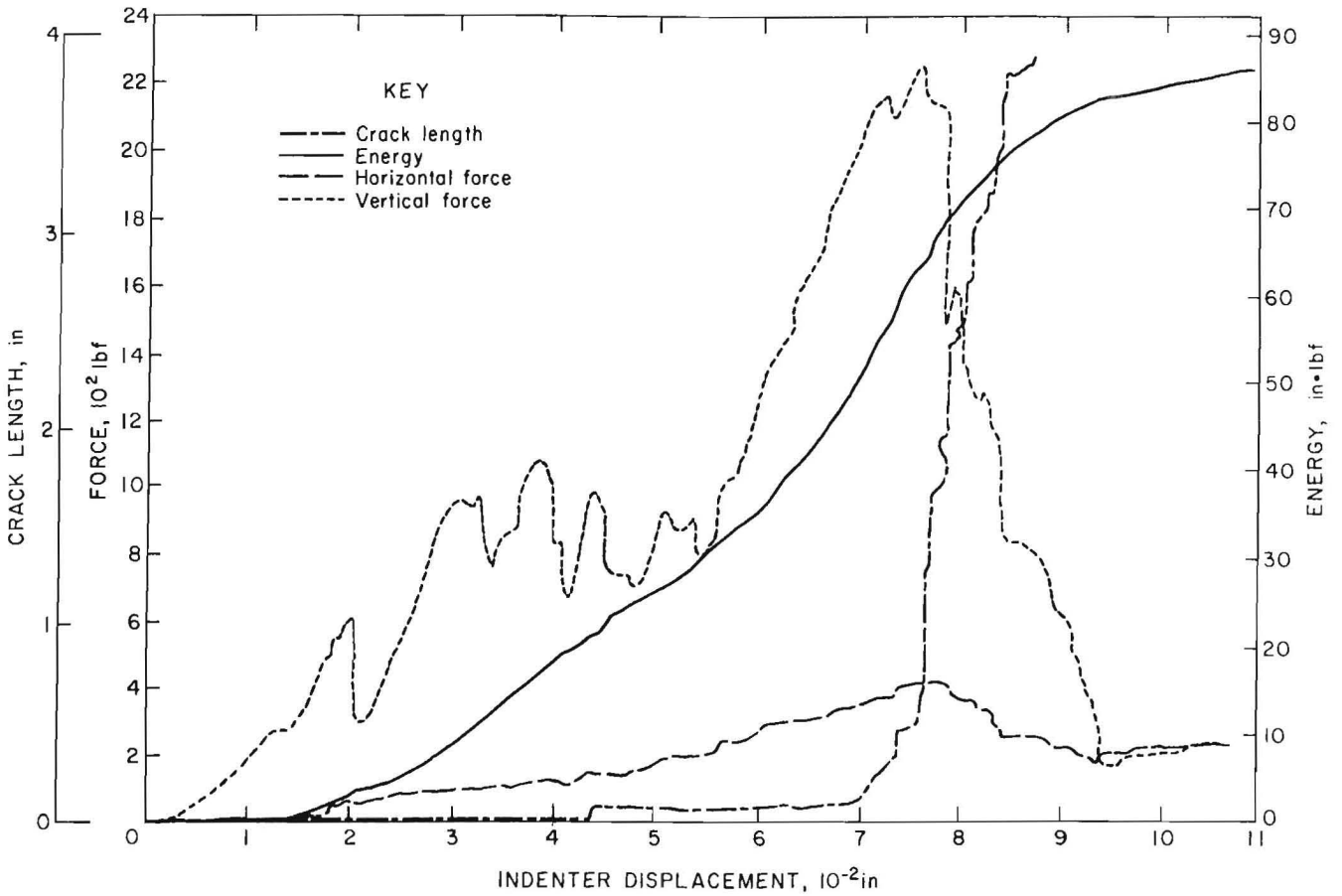

FIGURE 12.—Force, energy, and crack length as a function of indenter displacement for sample 10 splitting test.

A typical plot of vertical and horizontal forces, energy, and crack length as a function of indenter displacement is shown in figure 12.

EXPERIMENTAL RESULTS

The results of the splitting tests are shown in table 3 and figures 12 and 13. Again, the sequence of events leading up to total fracture of the sample was identical to that already described for the confined indentation tests. These were initial crushing, initiation of the crack, and stable growth of the crack. As before, small rock chips formed continuously to both sides of the indenter, resulting in a small crater with a crushed zone in the bottom.

The relationship between crack length and indenter load is shown in figure 13 for all the tests done. The short-dashed line simply connects the average of all of the tests while the solid and large-dashed lines represent the calculated forces, which will be discussed in the next section. The data show two distinct regions that correspond to the sequence of crushing and fracturing events. The first part of the curve involves the crushing phase and the initiation and growth of the crack up to about 1 in. In this region, the crack initiates and grows in response to the stress field under the indenter. According to Swain (11), it is the tensile component of the stress field that is of prime importance for brittle fracture of the type investigated in this report. Further, for the sharp indenters, the dominant tension develops immediately below the edge, which diminishes in a linear manner with distance along a downward-extending trajectory coincident with the loading direction. This predicts a crack to form near the tip of the bit and to grow

TABLE 3. - Splitting test data in Valders dolomite

Crack[1] length, in	Indenter displacement, 10^{-3} in	Vertical force, lbf	Cumulative energy, in·lbf
SAMPLE 9			
0.25...	50	941	23.4
0.5....	65	1,728	44.6
1.....	68	1,777	54.3
2.....	72	1,343	56.6
3.....	75	1,027	59.7
4.....	78	620	62.0
5.....	80	389	63.5
6.....	83	271	64.2
SAMPLE 10			
0.25...	31	1,038	12.4
0.5....	67	2,077	59.8
1.....	74	2,124	67.6
2.....	76	1,567	76.1
3.....	79	1,276	77.2
4.....	82	824	78.8
5.....	87	603	83.2
6.....	91	209	84.8

[1]Visual observations.

directly downward, which is confirmed in these experiments. The path of the fracture is somewhat erratic, tending to follow preexisting flaws or weaknesses in the rock, but generally follows the predicted paths.

The second region of crack growth ranges from about 1 to 6 in. The tip of the indenter is required to move approximately 0.1 in before region 2 begins. In this region, crack growth is caused by a simple wedging apart of the crack by the sides of the indenter or by the crushed rock beneath the tip of the indenter. In this region, crack extension is very efficient since the energy intensive crushing phase beneath the bit is eliminated. As the crack extends, the mechanical advantage of the wedge makes the vertical force more and more effective and the force required to extend the crack becomes less and less. Figure 14 shows schematically the two regions of crack growth experienced in these tests. Finally, the relationship between indenter load, F_v, and crack length and a comparison of maximum indenter load

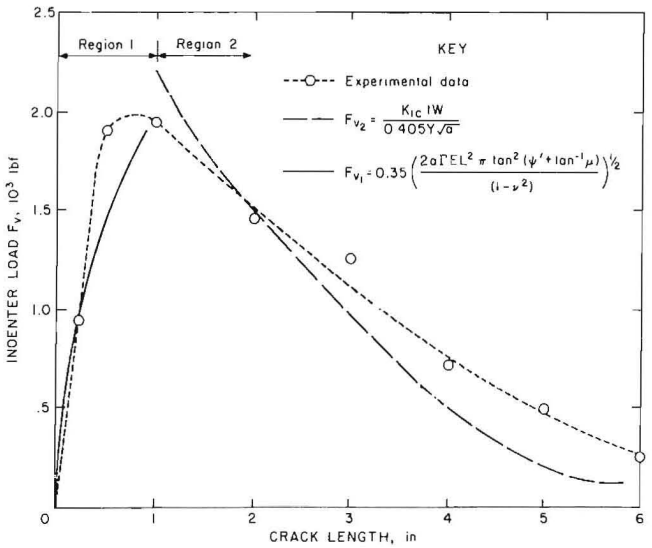

FIGURE 13.—Average indenter load (F_v) versus crack length for splitting test.

required to initiate fracture for the different test conditions will be made in the analysis section.

The energy required to form a unit area of fracture surface versus crack length is shown in figure 15. Note that 80 to 85 pct of the energy is used to initiate and drive the first 1 in of crack. This is because of the energy intensive crushing phase that is required to initiate the crack, the frictional losses between the bit and rock, and the energy going into chip formation. From about 1 in to 6 in (region 2), the energy required to fracture becomes less as the fracture extends. As noted earlier, this results from the efficient wedging action of the indenter, which becomes more effective as the crack extends. The specific surface energy of the process near the end of the test is close to the minimum theoretical fracture surface energy of the rock. For example, in sample 9 the specific surface energy from 5 to 6 in is 0.8 in·lbf/in^2, while the fracture surface energy for the rock is 0.25 in·lbf/in^2. Thus, the later stages of crack growth are very efficient and should be exploited as much as possible in mechanical cutting systems. A comparison of energy efficiencies for all systems tested will be done in the comparison section.

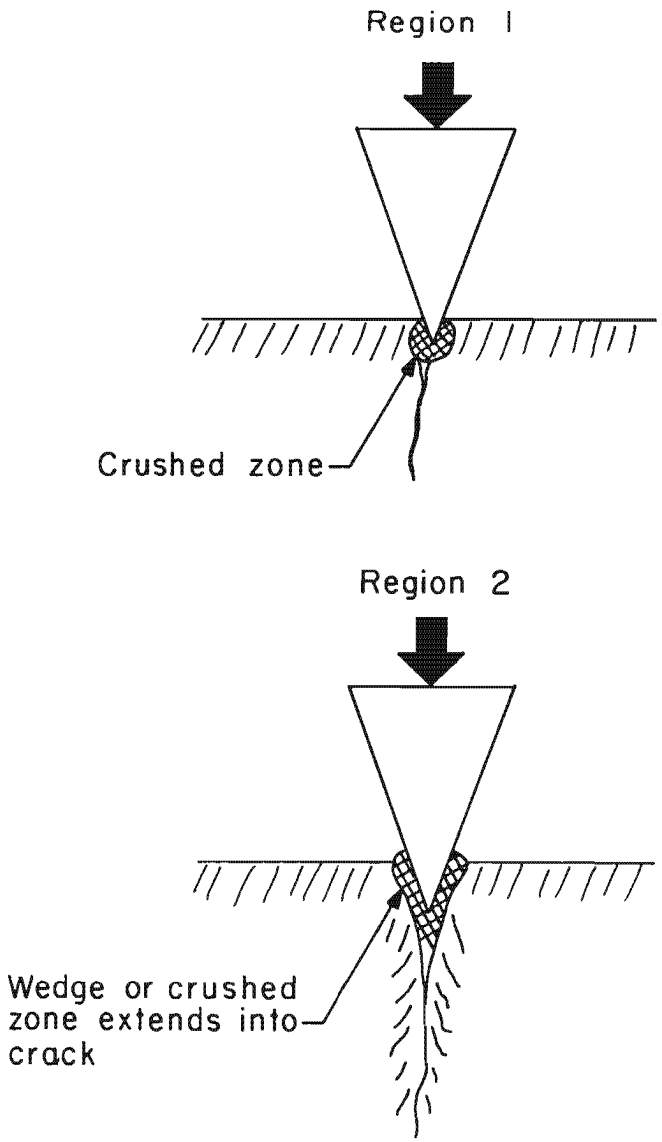

FIGURE 14.—Regions 1 and 2 of crack initiation and extension. In region 1, the crack extends because of the influence of tensile stress field under bit. In region 2, the crack extends because of the wedging action of the bit or crushed rock in the crack itself.

SPLITTING ANALYSIS

Because the fracture process for splitting shows two distinct regions of growth, it is necessary to analyze each separately. The first region (0 to 1 in) is complex, but is considered to be under the influence of the tensile stress field under the indenter. Thus, the Swain analysis used in the previous section was used to calculate indenter load as a function of crack length. The calculated loads, however, were very high and as a result equation 3 had to be modified to account for the lack of confinement of the splitting tests. Multiplying the equation by the constant (0.35) yielded values very close to the measured data. While this was considered sufficient for this preliminary report, more work needs to be done to analyze region 1. However, since the primary area of interest is the splitting process itself, the remainder of the analysis will deal exclusively with region 2.

Because region 2 is pure splitting, it lends itself to analysis using the stress intensity approach. To analyze this region, the stress intensity factor for the appropriate geometry is first determined. The geometrical representation of the splitting test setup is shown in figure 16 and the stress intensity is given by Hertzburg (17) as:

$$K_{IC} = Y \frac{F_H \, a^{1/2}}{tW}, \qquad (5)$$

where K_{IC} = stress intensity factor, psi $\sqrt{in}$,

Y = appropriate calibration factor for H/W = 0.5 and various a/W values,

F_H = applied load, lbf,

a = crack length, in,

t = thickness of sample (1 in),

and W = height of sample (6 in).

If K_{IC} can be calculated and substituted back into equation 5, then F_H can be solved for various values of crack length. Using the fact that

$$G_{IC} = 2\Gamma,$$

and

$$K_{IC} = \left| \frac{G_{IC} \, E}{(1-\nu^2)} \right|^{1/2},$$

K_{IC} can be calculated using $G_{IC} = 0.5$ in·lbf/in^2, $E = 5.7 \times 10^6$ lbf/in^2, and $\nu = 0.2$.

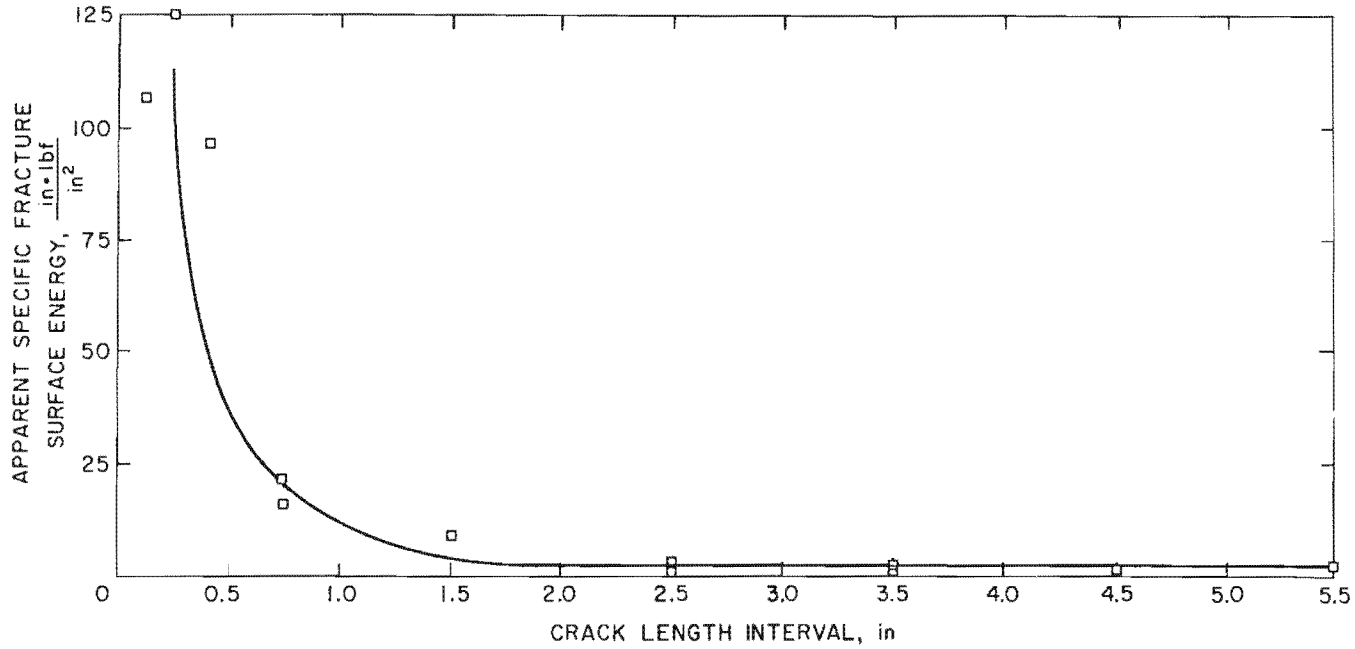

FIGURE 15.—Apparent specific fracture surface energy as a function of the crack length interval for splitting tests.

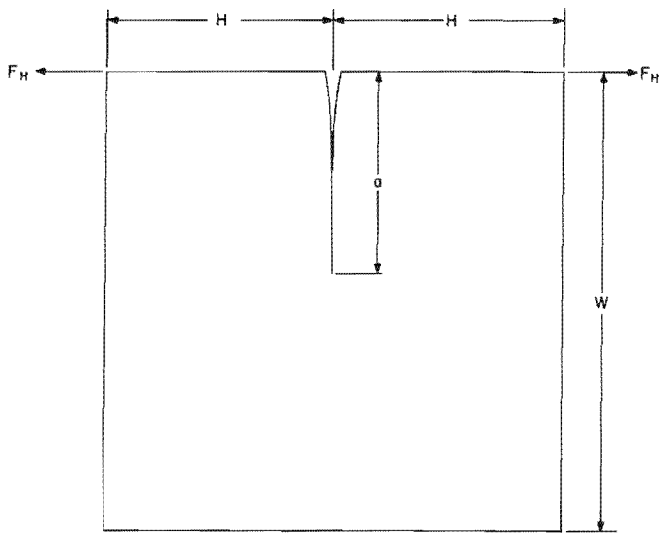

FIGURE 16.—Appropriate geometrical representation of region 2 splitting test. [After Hertzberg (17)]

With these values, K_{IC} equals 1.72 x 10^3 psi $\sqrt{in}$. Using this value of K_{IC}, F_H is then calculated as follows:

$$F_H = \frac{K_{IC}(t)(W)}{Y\sqrt{a}}, \qquad (6)$$

where F_H = horizontal indenter load component, lbf

t = sample thickness (1 in),

W = sample depth (6 in),

Y = calibration factor, which varies for a/W and H/W ratios [from Hertzberg (17)],

and a = crack length, in.

Since the force, F_H, is the horizontal component of the force applied by the wedge indenter, it is necessary to calculate the horizontal component of the wedge force. With the coefficient of kinetic friction of the bit against the rock as 0.6 (16), the analysis gives a horizontal force equal to 0.405 of the vertical force (see appendix) or

$$F_v = 2.47\ F_H, \qquad (7)$$

where F_v = vertical indenter load, lbf.

Figure 13 shows the crack length versus indenter load data and the calculated values from equations 6 and 7. The calculated values are within 16 pct of the measured data, which is considered

acceptable for this type of work. As noted earlier, the analysis does not apply to region 1. While equation 6 is not valid for a/W ratios larger than 0.7 or less than 0.2, Y calibration values were interpolated outside this range for the 1-in and the 5-in crack lengths. These interpolations yielded values that were also reasonable fits to the data and are shown in figure 13 as the long-dashed line. The close fit between the calculated and measured data show that the stress intensity approach is valid for the region 2 splitting process.

Finally, the splitting process in an unconfined sample represents the most efficient possible rock fracture with a wedge indenter. It represents an ideal to which other fracture processes can be compared. The next section will investigate a fragmentation system that tries to utilize this efficient region 2 fracture process by extending the median cracks to form large rock chips.

CHIPPING TESTS

The last series of tests performed in these experiments were the chipping tests. In these tests, the rock sample was confined and a layer of rock was removed by successive chipping. The chipping tests attempt to utilize the high efficiency of the stable crack growth stage to develop a more efficient fragmentation system for mechanical indenters. It should be noted that the chipping tests represent an idealized fragmentation system designed only to determine the advantages of using fracture to excavate rock. It is not being proposed as a commercial fragmentation system.

EXPERIMENTAL PROCEDURE

To simulate the free face of a previous cut, the 6- by 6- by 1-in-thick samples were notched 1/2 in deep, parallel to the bedding, with the bottom side of the diamond saw cut 2 in from the surface. The samples were tested with the bedding horizontal and positioned at the desired lateral spacing beneath the 40° wedge indenter. The sample was confined with a 1-in screw applying approximately 600 lbf against a steel load-distribution plate with thin, firm cardboard cushion between the steel and rock to prevent stress concentration. See figure 17 for the setup detail.

During testing, the loading rate was maintained at approximately 0.02 in/min to allow observation of the slow crack propagation. The average test duration was about 6 min. The forces, displacement, and crack extension were monitored. A typical plot of vertical force and energy is shown in figure 18.

EXPERIMENTAL RESULTS

The results of the chipping tests are summarized in table 4 and figures 19 and 20. The general sequence of chipping and the geometry of the chips are shown in figure 21. Because of the variations in rock properties and the shape of the adjacent free face, each rock chip was slightly different in size and in shape. However, all chips were generally parabolic in shape. The chips formed at the 1.0-in spacing were 2.5 times larger than those formed at the 0.5-in spacing, averaging approximately 0.055 lb in weight. The fracture surfaces were all generally flat and free of crushed material. The sequence of the fracturing events, starting with crack initiation and running through stable crack growth,

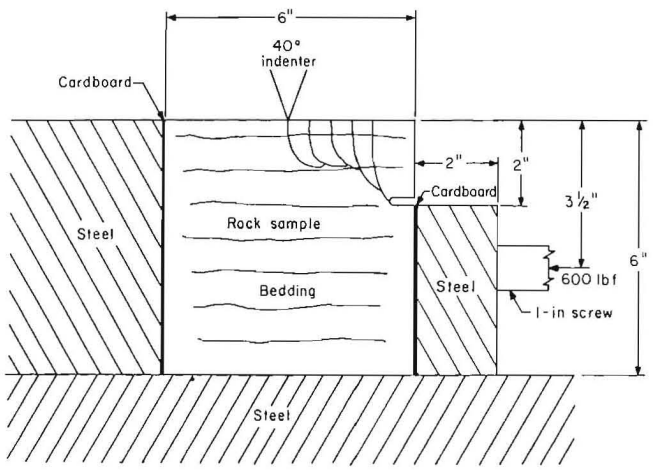

FIGURE 17.—Experimental setup for chipping tests.

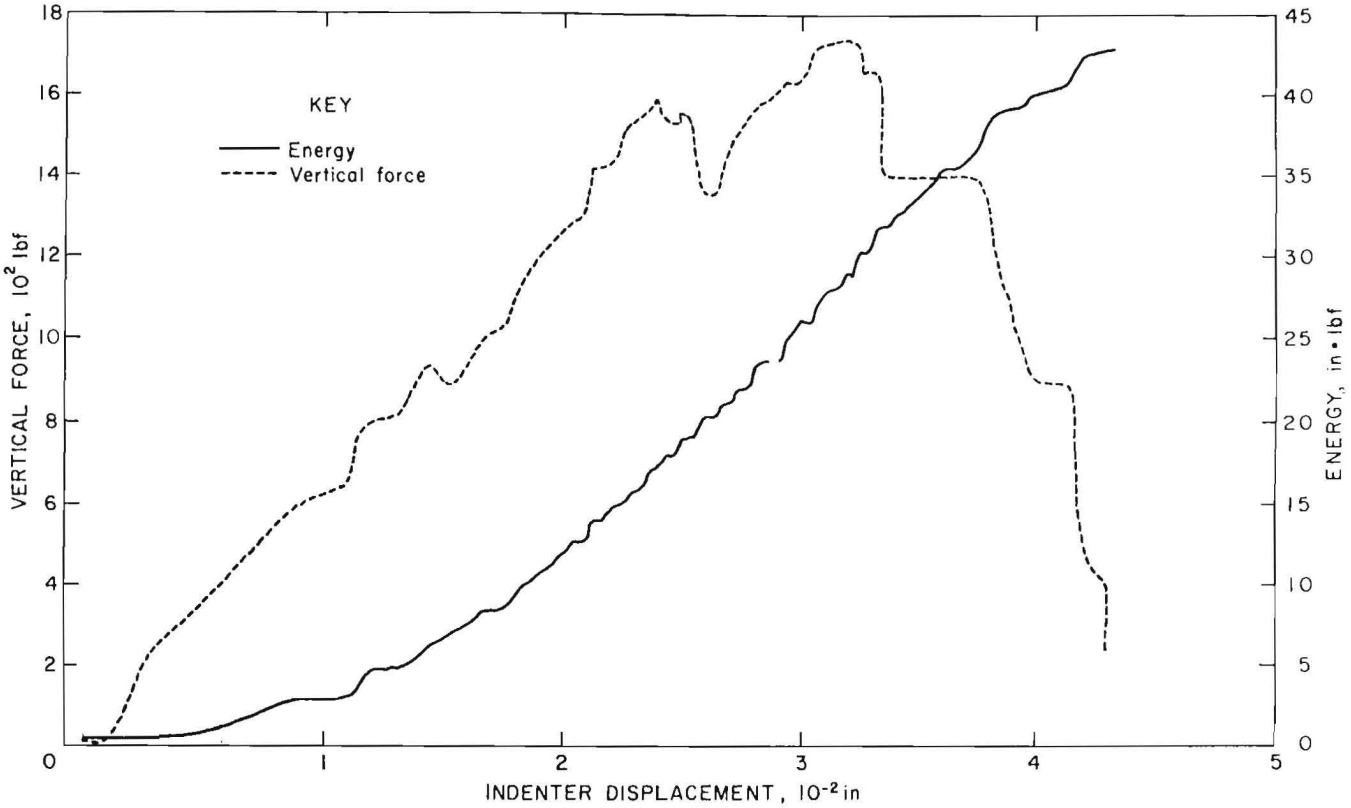

FIGURE 18.—Typical plot of vertical force and energy for the chipping tests.

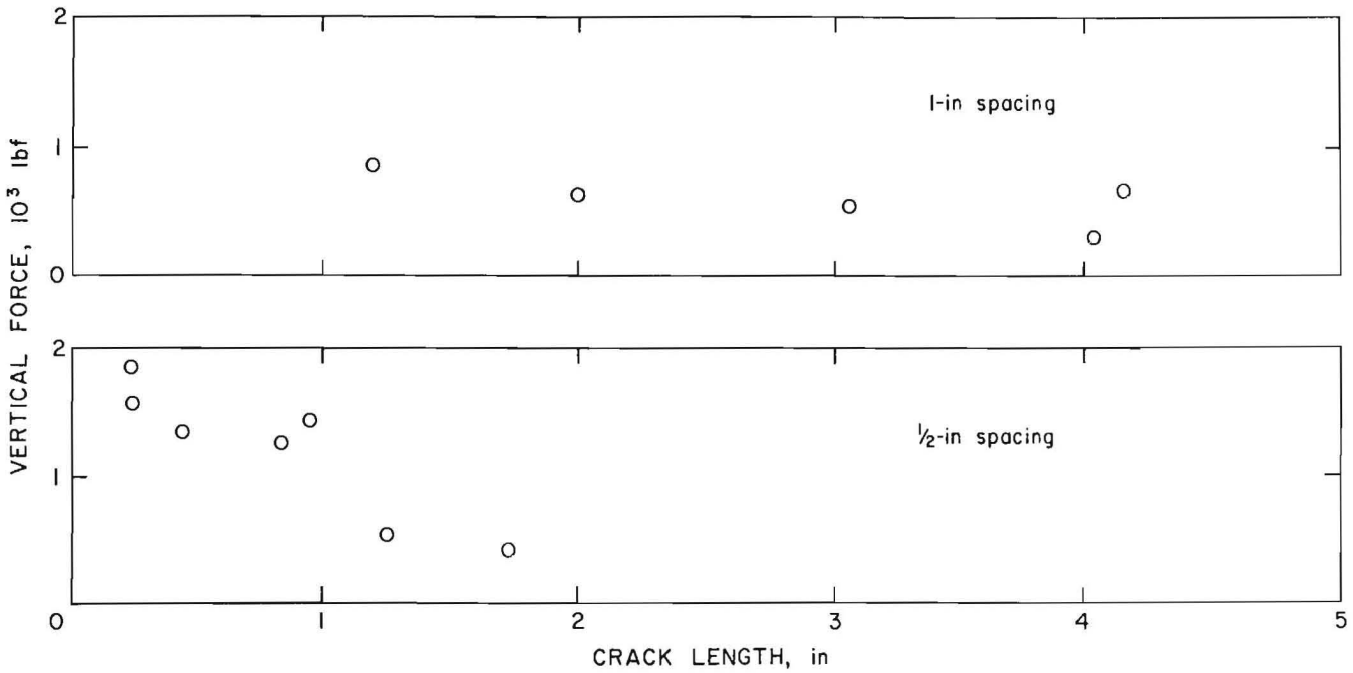

FIGURE 19.—Indenter force versus crack length for chipping tests (includes only data independent of edge influence).

was the same as that observed for both the indenting and the splitting tests.

The next result of interest is the relationship between indenter force and crack length. Figure 19 shows this relationship for 0.5- and 1.0-in spacings. Because of the variation in size of each chip, there is considerable scatter in the data. However, the trend for most tests showed the indenter force decreasing with increasing crack length, which is the same general result as seen for indenting and splitting. The peak forces required for the 1-in spacing are approximately 25 pct higher than for the 0.5-in spacing, as expected, and this result will be analyzed in the next section.

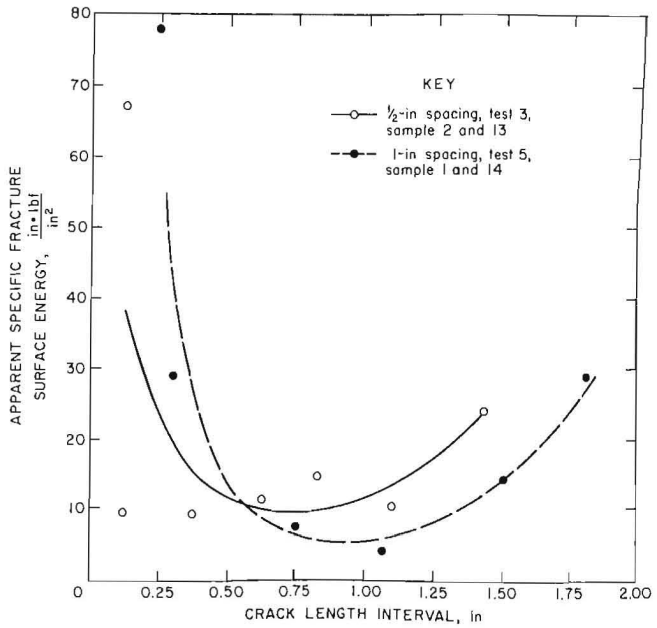

FIGURE 20.—Apparent specific fracture energy versus crack length interval.

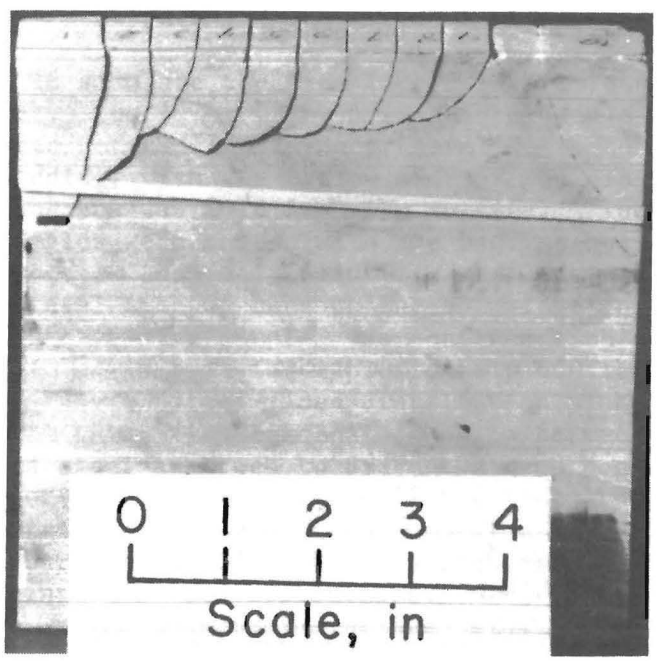

FIGURE 21.—Variation of chip shape for 0.5-in spacing.

Finally, the energy consumed in the chipping process is of interest. In general, the majority of the energy consumed during chipping was used in the first part of the process to initiate the crack. Again, this is the same result as seen previously and is a result of the need to crush the rock under the bit to initiate the crack. The specific surface energy of the process, therefore, varies over the sequence of fracturing events. Figure 20 shows the relationship between crack length and apparent specific fracture surface energy. Note that the surface energy is very high at the crack start, then decreases to a minimum, and finally, increases slightly near the end of the process. The increase at the end of the process results from the change in the fracture path from straight to curved, which is more difficult to drive. The difference in fracture surface energies between the 0.5- and 1.0-in spacings is not apparent from the data. However, more tests will be required to confirm this result.

CHIPPING ANALYSIS

The problem of predicting the force required to fracture off a corner of a block is best handled by the energy release rate analysis rather than by the stress field approach used in the last two sections. This is because the stress field under an indenter near a curved free face is not well understood and the relative dimensions of the chip need to be introduced. The energy release rate was used by Kaplan (18) to predict the maximum force required to form a chip, starting from a predrilled hole and extending up to the surface, with good results. The same method is used here to

TABLE 4. - Chipping test data in Valders dolomite

Run	Spacing from last run or edge of sample, in	Peak vertical force during test, lbf	Crack[1] length, in	Indenter displacement, 10^{-3} in	Vertical force, lbf	Cumulative energy, in·lbf
SAMPLE 1, 1.05-in THICK						
1.....	0.9	NA	1.93	NA	NA	NA
2.....	.5	1,449	1.25	19	947	12.8
			1.88	33	178	17.8
3.....	.5	1,081	.50	34	1,070	9.7
			1.00	37	685	12.6
			1.38	57	238	20.6
4.....	.5	2,195	.50	15	1,935	7.3
			1.00	18	1,840	15.2
			1.85	35	539	45.3
5.....	.5	1,750	.25	24	1,591	17.6
			.5	26	1,367	20.1
			1.15	32	1,750	30.1
			1.70	43	418	43.0
6.....	.5	1,457	.10	24	1,122	14.7
			.94	28	1,440	21.8
			1.40	45	309	32.0
7.....	.5	1,940	.25	23	1,547	13.4
			.88	30	1,775	26.4
			1.45	42	679	44.0
8.....	.5	1,857	.25	24	1,857	23.8
			.83	29	1,282	28.1
			1.25	40	556	42.3
9[2].....	.5	2,618	.25	32	2,128	41.4
			1.21	44	925	68.0
SAMPLE 14, 1.00-in THICK						
1.....	0.8	1,000	0.25	41	861	6.1
			1.50	45	1,000	9.2
			2.12	55	32	10.0
2.....	.5	682	.25	17	629	3.2
			1.00	20	337	5.2
			1.14	36	188	8.0
3.....	.5	1,682	.25	13	1,258	6.9
			1.00	20	1,506	16.7
			2.62	40	198	27.0
4.....	.5	1,032	.25	14	894	5.4
			1.00	18	978	10.0
			1.52	29	86	13.0

See explanatory notes at end of table.

TABLE 4. - Chipping test data in Valders dolomite--Continued

Run	Spacing from last run or edge of sample, in	Peak vertical force during test, lbf	Crack[1] length, in	Indenter displacement, 10^{-3} in	Vertical force, lbf	Cumulative energy, in·lbf
SAMPLE 2, 0.94-in THICK						
1.....	1.0	1,881	0.83	22	814	18.1
			[3]1.11	24	526	19.0
			[4]2.10	25	251	19.8
	1.0	2,937	[3].16	57	2,892	49.5
			[3].79	72	2,226	74.0
			[3]2.50	77	2,346	96.6
			[4]3.46	113	756	151.0
3.....	1.0	1,531	[3].60	18	859	16.3
			[3]1.53	50	579	20.0
			[3]2.08	54	684	35.0
SAMPLE 13, 1.00-in THICK						
1.....	1.0	1,566	0.25	52	1,313	37.9
			1.00	76	1,558	82.3
			2.20	84	176	86.9
2.....	1.0	2,441	1.00	111	622	93.9
			2.02	134	299	101.0
3.....	1.0	2,104	.50	72	2,104	39.0
			1.00	79	1,891	42.8
			2.00	126	1,716	57.3

NA Not available.

[1]Visual observations on front surface; final crack length for each run is average length formed along chip.

[2]0.7-in vertical crack developed before a branch ran to the free face.

[3]Grid measure crack length.

[4]Measured chip surface.

predict the maximum force required to form an edge chip. It is assumed that the edge chip can be modeled by a cantilevered beam as shown in figure 22. The strain energy release rate of this cantilevered beam is then equated to the experimentally determined critical energy release rate and the load required to fracture the rock can be calculated. In general, the strain energy release rate per unit thickness is given by

$$G = \frac{\delta U}{\delta a}, \qquad (8)$$

where G = strain energy release rate, in·lbf/in^2,

U = elastic strain energy in rock, in·lbf,

and a = crack length, in.

The strain energy in a cantilevered beam subject to a concentrated force is given as

$$U = \frac{F_H{}^2 a^3}{2EI}, \qquad (9)$$

where F_H = force acting on the end of the beam, lbf,

E = Young's modulus, lbf/in^2,

and I = moment of inertia, in^4.

Then

$$\frac{\delta U}{\delta a} = \frac{3F_H{}^2 a^2}{2EI}.$$

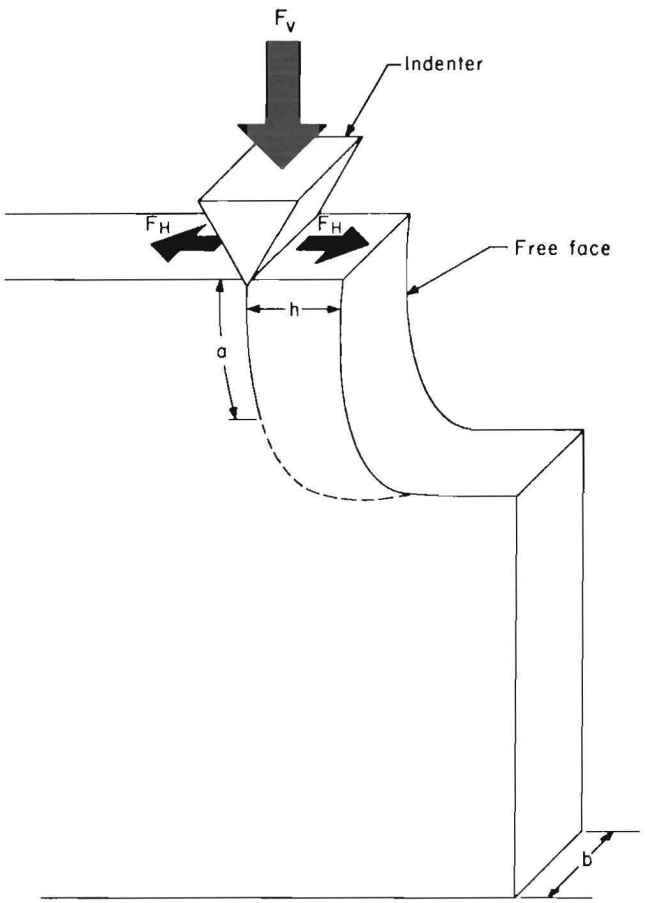

FIGURE 22.—Geometry of chip process.

Substituting $I = bh^3/12$ for a rectangular beam and equating to G yields

$$G = 18 \frac{F_H^2 a^2}{Ebh^3},$$

and finally solving for the force F_H yields

$$F_H = \left| \frac{GEbh^3}{18a^2} \right|^{1/2}. \qquad (10)$$

F_H is the force applied to the rock perpendicular to the surface of the fracture. Assuming a coefficient of friction between the wedge and the rock of 0.6, the calculated the vertical force applied to the wedge is

$$F_V = 2.47\ (F_H). \qquad (11)$$

By using equations 10 and 11, the maximum vertical force required to fracture was calculated to be 1,389 lbf for the 1/2-in and 3,931 lbf for the 1-in spacing. This compares to the average peak experimental forces of 1,565 and 2,076 lbf, respectively. The calculated value for the 1/2-in spacing is reasonable, but is not for the 1.0-in spacing. The difficulty may be in modeling the chip as a cantilevered beam that is subjected only to a bending stress. This analysis leads to the indenter load being a function of spacing raised to the 3/2 power. The 1-in data do not follow this 3/2 power rate, but rather appear to follow a power of 1 or less.

To better match the data, a second analysis was performed that modeled the chip as a cantilevered beam, but subject only to a shear stress. This seemed more reasonable given the short length of the chip at the beginning of the fracturing process. Consequently, the shear strain energy for a beam was calculated and the change in this strain energy as a function of crack length was equated to the critical strain energy release rate to yield the following relationship for F_H:

$$F_H = \left| \frac{5GSbh}{3} \right|^{1/2}, \qquad (12)$$

where S = shear modulus of elasticity (2.55×10^6 lbf/in^2).

Using equations 12 and 11, the vertical force for the 1/2-in spacing was calculated at 2,546 lbf and for the 1.0-in spacing at 3,600 lbf. Although the calculated values are somewhat worse at the 1/2-in spacing, they are better at the 1-in spacing. Moreover, the force is related to the spacing raised to the 1/2 power, which seems to fit the data better than the previous analysis. Therefore, while the strain energy release rate type of analysis appears promising, more data will be required before the exact force versus spacing relationship can be defined.

Finally, for the chipping type fracture tests, the path of the crack is also of interest. The path of a crack near a corner is known by experience to be curved. The exact path, however, is governed by the stress field induced by the wedge indenter. According to Lawn (9), the path of the fracture will be determined by that which maximizes the quantity $G-2\Gamma$. G is the mechanical energy release rate and Γ is the fracture surface energy of a solid. In an ideally brittle material, the fracture surface energy, Γ, reduces to the surface energy. In practice, the crack tends to propagate along trajectories of lesser principal stress in the prior field, thereby maintaining near orthogonality to a major component of tension. Thus, if the stress field is known prior to crack propagation, the path can be calculated.

For the case of a wedge indenter near a free face, the stress field has been determined from photoelastic studies by Garner (19). The locus of maximum tensile stress is shown in figure 23 and shows a potential fracture plane that extends from the rock bit interface toward the bottom of the free face. This is confirmed by the laboratory results of the report, which show the curved crack path to the free surface. Note that Garner's stress field applies only to the first chip and the vertical free face. The succeeding chips are formed to intersect a curved free face, which tends to decrease the length of the crack. Because of the importance of the stress field on the direction of the fracture, this area will be investigated in more detail in future work.

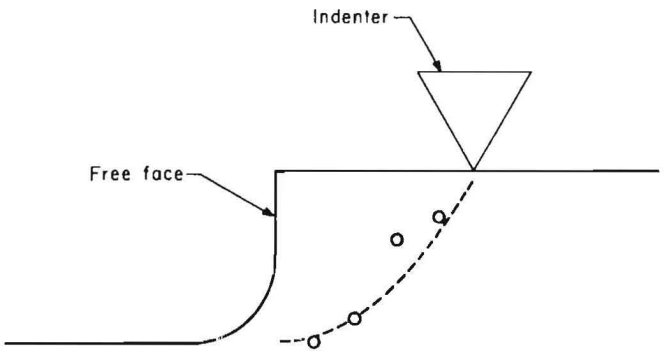

FIGURE 23.—Locus of maximum tensile stress for a wedge indenter near a free face. [Adapted from Garner (19)]

Finally, it should also be recognized that the crack path is also influenced by the anisotropy of the rock itself. In general, the crack path will propagate along the easiest low-energy paths such as following existing flaws, fractures, and other structural weaknesses. Therefore, the crack path can never be predicted with exactness in the real non-isotropic situation. However, it is the ultimate goal of this work to be able to direct the crack path in such a manner as to maximize chip volume produced per fracture energy expanded.

COMPARISON OF METHODS

In this section the force required to initiate and extend a crack and the energy efficiency of the fracture process will be compared for all three test conditions or methods. Since the chipping method is an actual volume removal process, it will also be compared with other mechanical fragmentation systems in the same rock.

Figure 24 shows the theoretical indenter force versus crack length relationship for all three methods tested. The data for the chipping tests are very limited, from 0 to 0.25 and 0 to 0.5 in for the 1/2-in and 1-in spacing, respectively. Therefore, the theoretical curve is shown dashed to indicate that the relationship is assumed.

The relationships for the indentation and splitting methods are similar in the initial stages of fracture. That is, the indenter force required to fracture increases as a function of the square root of crack length up to a maximum value, after which the indenter force decreases with increasing crack length. Since the pure indentation method cannot form a chip, the force does not reach a peak value, but simply increases as a function of the crack length raised to the 1/2 power. The value of peak force required for the splitting and chipping methods

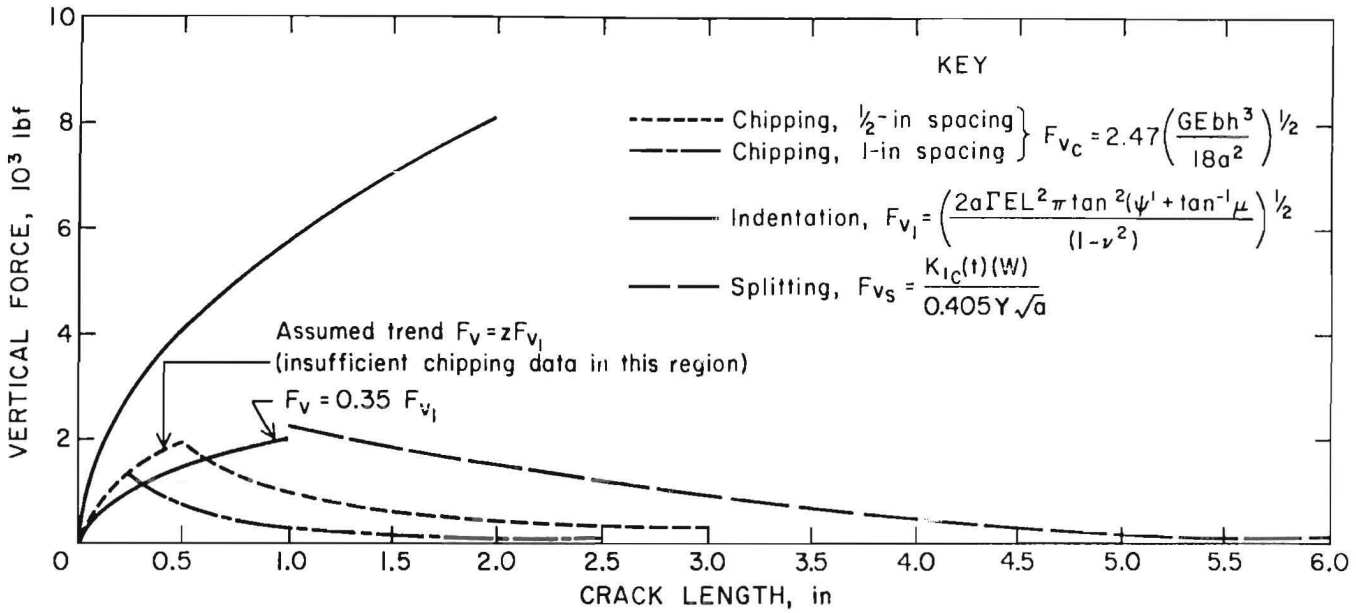

FIGURE 24.—Theoretical indenter force versus crack length for the indentation, splitting, and chipping methods.

depends upon the strain energy in the chip and hence the geometry of the chip. Therefore, the 1/2-in spacing (with a smaller chip) requires a lower peak force than the 1-in spacing (with a larger chip) and both require less than the splitting method, which can be thought of as having a 3-in spacing.

Once the peak force is reached, the crack is simply wedged apart by the indenter and the mechanical advantage of the system increases as the crack length increases. Thus, the indenter force falls off as a function of the crack length, reaching very low values. This region achieves very efficient fracture and should be maximized to achieve high-efficiency fragmentation.

Figure 25 shows the apparent specific fracture surface energy as a function of crack length. Specific fracture surface energy is defined as the energy required to create a unit area of fracture surface. As seen in figure 25, this is not a constant, but varies with crack length. It approaches a steady-state value as crack length increases with the exception of the chipping tests. The specific energy of chipping begins to increase near the end of the chip because of the change in direction of the crack and the less efficient wedging action of the indenter. In general, however, all methods achieve a very low specific fracture energy approaching the theoretical limit, which is the surface energy of the material. Thus, rock fracture with an indenter is an efficient method of driving cracks, especially as the crack length exceeds approximately 1 in. The indentation method required the highest specific fracture surface, as expected, because of the confinement of the sample. The chipping achieved slightly better specific energy than the splitting method in the first part of the crack, but eventually became less efficient as the curved part of the chip was formed. Beyond about 1.5 in the splitting method achieved the best specific fracture energy of all methods

Since the chipping method also represents a volume removal system, it can be compared with other excavation systems. In this case, the specific energy or energy to remove a unit volume of rock is used as the basis of comparison. In these chipping tests, specific energies as low as 25 in·lbf/in^3 were achieved. For comparison, the best specific energy obtained for a drag cutter was 2,385 in·lbf/in^3 (1) and for a disk cutter was approximately 4,000 in·lbf/in^3. Thus, the chipping is up to 100 times more

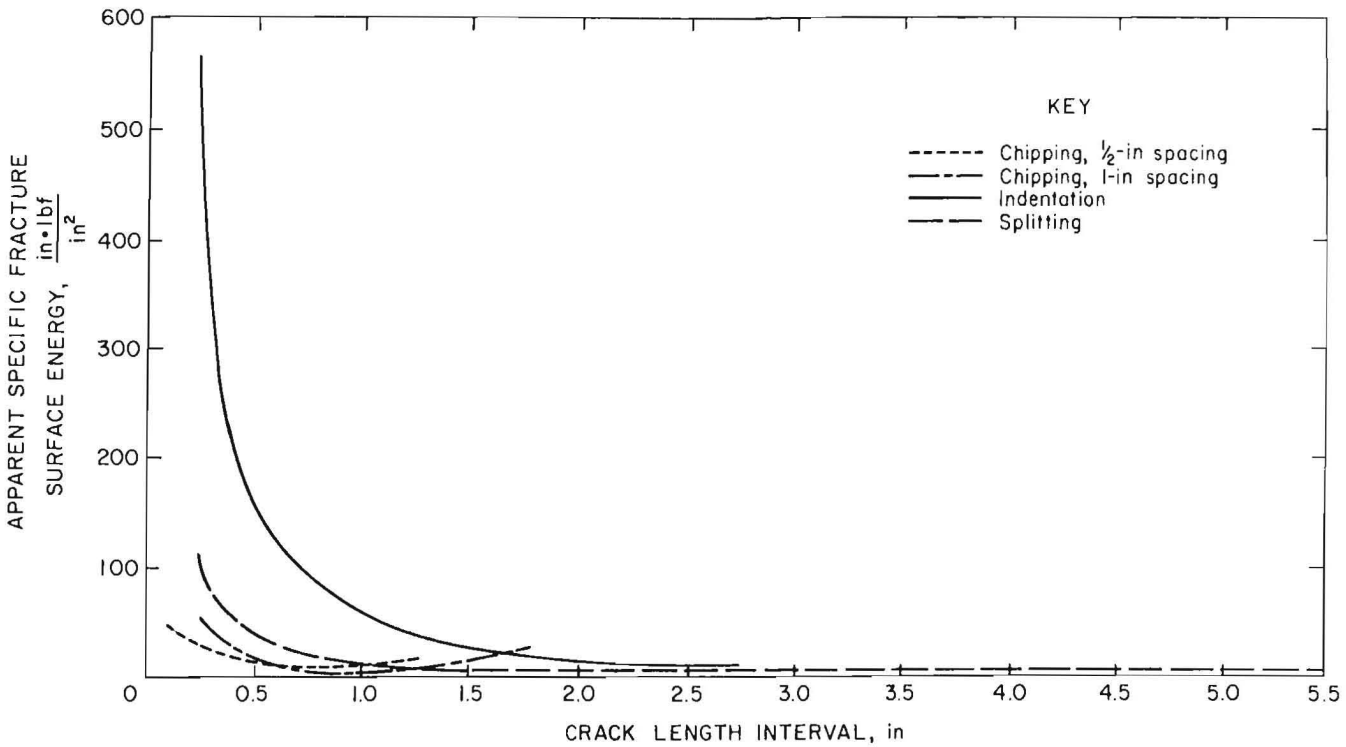

FIGURE 25.—Specific fracture surface energy as a function of crack length for the indentation, splitting, and chipping methods.

efficient than conventional methods. However, since the chipping was done essentially in plane stress conditions, it is anticipated that the specific energy will increase when used in the more confined plane strain conditions. As noted earlier, chipping is an idealized method used to illustrate the controlled fracture process and is not being proposed as a viable fragmentation system.

CONCLUSIONS

Experiments with wedge indenters under plane stress conditions has shown that long subsurface cracks form under the tip of the indenter and that these cracks can be propagated in an energy efficient manner to form rock chips. The energy required to drive these cracks approaches the surface energy of the rock for long cracks in an unconfined sample. This type of controlled fracture has the potential to provide large improvements in excavation technology. Edge chipping, which is an idealized controlled fracture process, achieved energy efficiencies approximately 100 times better than conventional methods. Most of this improvement results from the elimination of the sliding contact between the bit and the rock and the elimination of excess fragmentation of the rock. Thus controlled fracture greatly reduces the problems of frictional energy losses, rapid bit wear, and the generation of hazardous dust and fines normally encountered in conventional mechanical fragmentation systems. Because of the great potential of controlled fracture in mechanical fragmentation, more experiments will be performed with this method.

REFERENCES

1. Morrell, R. J., D. A. Larson, and D. E. Swanson. Large-Scale Laboratory Drag Cutter Experiments in Hard Rock. BuMines RI 9003, 1986, 18 pp.

2. Anderson, S. J., and D. E. Swanson. Laboratory Testing of a Radial-Axial Loading Splitting Tool. BuMines RI 8722, 1982, 26 pp.

3. Friedman, M., and L. M. Ford. Analysis of Rock Deformation and Fractures Induced by Rock Cutting Tools Used in Coal Mining. Paper in Proceedings of 24th U.S. Symposium on Rock Mechanics (Texas A&M Univ., June 20-23, 1983). 1983, pp. 713-723.

4. Zeuch, D. H., D. V. Swenson, and J. T. Finger. Subsurface Damage Development in Rock During Drag-Bit Cutting: Observations and Model Prediction. Paper in Proceedings of 24th Symposium on Rock Mechanics (Texas A&M Univ., June 20-23, 1983). 1983, pp. 733-742.

5. Tutluoglu, L., M. Hood, and C. Barton. An Investigation of the Mechanisms of Water Jet Assistance on the Rock Cutting Process. Paper in Proceedings of the 20th Symposium on Rock Mechanics (Texas A&M Univ., College Station, TX, June 20-23, 1983). 1983, pp. 743-749.

6. Hood, M. A Study of Methods To Improve the Performance of Drag Bits Used To Cut Hard Rock. Chamber of Mines of South Africa, Johannesburg, South Africa, Rep. 35177, Proj. GT2, No. 2, Aug. 1977, 135 pp.

7. Lundquist, R. G. Rock Drilling Characteristics of Hemispherical Insert Bits. M.S. Thesis, Univ. of Minnesota, Minneapolis, MN, Jan. 1968, 88 pp.

8. Tandanand, S. Principles of Drilling. Sec. in SME Mining Engineering Handbook. Soc. Min. Eng. AIME, v. 1, 1973, pp. 11-5--11-13.

9. Lawn, B. R., and R. Wilshaw. Review Indentation Fracture: Principles and Applications. J. Mater. Sci., v. 10, 1975, pp. 1049-1081.

10. Lawn, B. R., and M. V. Swain. Microfracture Beneath Point Indentions in Brittle Solids. J. Mater. Sci., v. 10, 1975, pp. 113-122.

11. Swain, M. V., and B. R. Lawn. Indentation Fracture in Brittle Rocks and Glasses. Int. J. Rock Mech. Min. Sci. & Geomech. Abstr., v. 13, 1976, pp. 311-319.

12. Griffith, A. A. The Phenomena of Rupture and Flow in Solids. Phil. Trans. Royal Soc. of London, A221, 1920, p. 163.

13. Irwin, G. R. Fracture. Sec. in Handbook der Physik. Springer-Verlog, 1958, v. 6, p. 551.

14. Smirnov, V. V. A Method of Measuring the Crack Propagation Velocity in a Rock Specimen Under Impact Load. Sov. Min. Sci. (Engl. Transl.), v. 3, May-June 1968, pp. 260-263.

15. Ellis, R. C. Evaluation of Effective Fracture Energy of Valders Limestone by Two-Level Factorial Design. M.S. Thesis, Univ. of Wisconsin, Madison, WI, Jan. 1968, 81 pp.

16. Tuma, J. J. Statics, ed. by J. Schaune, M. Schaum, R. Meltzer, and G. Lobell. Quantum Publ., Inc., 1974, p. 225.

17. Hertzberg, R. W. Deformation and Fracture Mechanics of Engineering Materials. Wiley, 2d ed., 1983, p. 281.

18. Kaplan, M., and D. Chazin. Potential Applications of Drill-Split Fragmentation Systems in Underground Mines (contract J0285016, Sci. Applications, Inc.). BuMines OFR 86-80, 1979, 188 pp.; NTIS PB 80-210792.

19. Garner, N. E. The Photoelastic Determination of the Stress Distribution Caused by a Bit Tooth on an Indexed Surface. M.S. Thesis, Univ. of Texas, Austin, TX, Jan. 1961, 57 pp.

APPENDIX.--WEDGE ANALYSIS

$$\sum Fy = \frac{F_v}{2} - N_{Lv} - f_{Lv} = 0,$$

$$\frac{F_v}{2} - N_L \sin\theta - f_L \cos\theta = 0,$$

$$\frac{F_v}{2} - N_L \sin\theta - \mu N_L \cos\theta = 0,$$

$$\frac{F_v}{2} = N_L (\sin\theta + \mu \cos\theta),$$

$$N_L = \frac{F_v}{2 (\sin\theta - \mu\cos\theta)},$$

and total left side horizontal force, $F_H = N_{LH} - f_{LH}$.

$$F_H = N_L \cos\theta - f_L \sin\theta,$$

$$F_H = N_L \cos\theta - \mu N_L \sin\theta,$$

$$F_H = N_L (\cos\theta - \mu \sin\theta).$$

Substituting $N_L = F_v/2 (\sin\theta - \mu \cos\theta)$,

$$F_H = \frac{F_v (\cos\theta - \mu \sin\theta)}{2 (\sin\theta + \mu \cos\theta)},$$

when $\theta = 20°$, $\mu = 0.6$,

$$F_H = 0.405\ F_v.$$

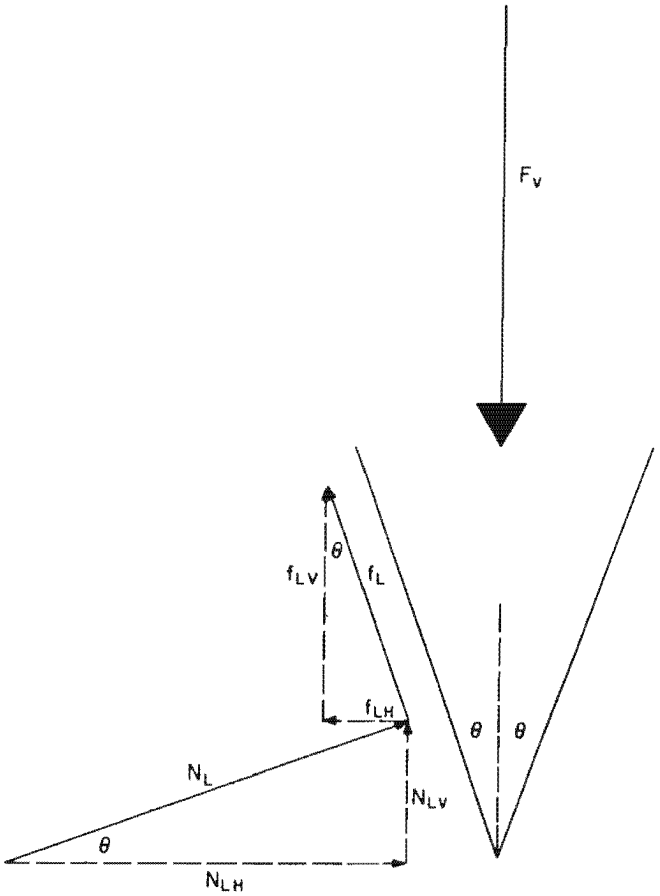

FIGURE A-1.—Wedge force analysis.

U.S. GOVERNMENT PRINTING OFFICE: 1987 - 605-017/60069

INT.-BU.OF MINES,PGH.,PA. 28525